Monitoring Neural Activity with Bioluminescence during Natural Behavior

Monitoring Neural Activity with Bioluminescence during Natural Behavior

Eva A. Naumann*, Adam R. Kampff *, David A. Prober, Alexander F. Schier and Florian Engert

*equal contribution

Department of Molecular and Cellular Biology, Center for Brain Science, Harvard University,

16 Divinity Avenue, Cambridge MA, 02138, USA

Correspondence:

Florian Engert

Department of Molecular and Cellular Biology

Harvard University, Biolabs Room 2073

16 Divinity Avenue,

Cambridge MA 02138

Tel: 617-495-4382

Email: florian@mcb.harvard.edu

Abstract

Existing techniques for monitoring neural activity in awake, freely behaving vertebrates are invasive and difficult to target to genetically identified neurons. Here we describe the use of bioluminescence to non-invasively monitor the activity of genetically specified neurons in freely behaving zebrafish. Transgenic fish expressing the Ca^{2+}-sensitive photoprotein GFP-apoAequorin (GA) in most neurons generated large and fast bioluminescent signals related to neural activity, neuroluminescence, that could be recorded continuously for many days. To test the limits of this technique, GA was specifically targeted to the hypocretin-positive neurons of the hypothalamus. We found that neuroluminescence generated by this group of ~20 neurons was associated with periods of increased locomotor activity and identified two classes of neural activity corresponding to distinct swim latencies. Thus, our neuroluminescence assay can report, with high temporal resolution and sensitivity, the activity of small subsets of neurons during unrestrained behavior.

Key words:

***in vivo* neural recording; behavior; genetically encoded calcium indicator; zebrafish; Aequorin**

To correlate the activation of specific neurons with the execution of specific behaviors, it is necessary to monitor neural activity while an animal behaves. Neural recordings in freely moving animals are possible with electrophysiology, but the available techniques are invasive, often cannot target specific neurons, and are restricted to organisms that can physically transport the required electronics [1-2]. Optical techniques, using genetic strategies to target protein reporters to specific neurons and non-invasively monitor their activity, provide a promising alternative [3]. These tools have provided access to neurons in the larval zebrafish brain and allow monitoring and manipulating their activity *in vivo* [4-8]. In particular, synthetic and genetically-encoded fluorescent Ca^{2+}-indicators, targeted to distinct neural populations, have been

used to relate the activity of defined cell-types to different stimuli or behaviors [9-11]. However, fluorescence imaging strategies used to optically detect neural activity are selective for signals arising from a narrow focal plane, and these signals are corrupted when motion causes fluorescently-labeled neurons to enter and exit the imaged region [8,12]. This sensitivity to movement has limited imaging techniques to restrained, paralyzed or anesthetized animals for which behavior is abolished or severely restricted [10,13-14].

In principle, a "non-imaging" technique can allow monitoring neural activity in freely behaving zebrafish. Non-imaging systems do not attempt to form an image of the source at the light detector and thus do not require intermediate focusing optics. As a consequence, a large-area photo-detector can be positioned directly above the behavior arena. The detector receives light emitted from anywhere within the arena and the optical signals from the neurons labeled in a translucent organism are unaffected by the animal's movement throughout the collection volume. Although this approach sacrifices all spatial information, a conventional imaging approach will also suffer from a loss of spatial information when used with freely behaving animals: emitted light is scattered by intact tissue and movement of the labeled neurons out of the focal plane will severely limit the possible spatial resolution. In addition, natural behavior requires an arena size substantially larger than the animal and, unless behavior is slow enough to allow the imaging setup to accurately move along with the animal[15], the entire area must be imaged at high resolution to gain useful spatial information, all while maintaining the high frame rates necessary for monitoring activity on physiologically relevant timescales. Given the limited spatial information available to an imaging assay of behaving animals, we decided to pursue a non-imaging approach, which is technically straightforward, inexpensive, provides higher temporal resolution, and is able to detect a large portion of emitted light because the detector can be installed close to the behavior arena. Furthermore, spatial information can be gained indirectly by using a genetically-encoded reporter and targeting its expression only to the neurons of interest [3]. A non-imaging detection system with a genetically-encoded neural activity

reporter would provide a powerful new tool for selectively recording from genetically-defined neurons during natural behavior.

Unfortunately, two features of the commonly-used fluorescent activity reporters preclude their use in a non-imaging setup. First, most fluorescent Ca^{2+}-indicators have baseline light emission when unbound to Ca^{2+} and, regardless of this basal fluorescence, auto-fluorescence will provide a significant background signal. With these sources of background emission, any changes in excitation or detection efficiency caused by motion within the collection volume will produce changes in the detected fluorescence unrelated to neural activity. Second, the use of fluorescent indicators in a non-imaging setup requires an intense visible excitation light to homogenously fill the behavior/collection arena. In addition to the technical challenge, this excitation light would also disrupt assays of vision and might confound other behavioral experiments (e.g. studies of sleep).

In contrast to fluorescent reporters, Aequorin, a Ca^{2+}-dependent bioluminescent protein produced by the jellyfish *Aequorea Victoria* , has no background light emission at basal Ca^{2+} levels and does not require excitation light. Based on these properties alone, we reasoned that Aequorin might be well suited for non-imaging assays of neural activity in freely moving zebrafish. Furthermore, Aequorin has demonstrated excellent characteristics as a genetically-encoded Ca^{2+}sensor [16]. Upon binding calcium, Aequorin (luciferase) catalyzes the completion of the luciferase reaction, the oxidation of its substrate (luciferin) coelenterazine (CLZN), resulting in the production of a blue photon [17]. Purified Aequorin has been employed as an optical indicator of intracellular Ca^{2+} in many cell-types, including neurons [18-19]. In jellyfish, Aequorin naturally occurs as a complex with green-fluorescent protein (GFP), and via a process termed chemiluminescence resonance energy transfer (CRET), the energy from CLZN oxidation is transferred to GFP and results in the emission of a green photon [20]. The efficiency of Ca^{2+}-dependent photoemission from Aequorin is enhanced when associated with GFP (from 10% to 90%), which inspired the development of a GFP-Aequorin fusion (GA) [16]. GA retains the fast kinetics of Aequorin (6-30 ms rise

time [21]) and its sensitivity to Ca^{2+}-concentrations ranging from 100 nM–10 μM [22], which is on par with the best synthetic Ca^{2+} sensors. In addition, the associated GFP provides a fluorescent tag that can be imaged with conventional fluorescence methods to localize and quantify GA expression. These improved features of GA have fostered new interest in bioluminescence assays for neural Ca^{2+} signals and it has been successfully employed to monitor pharmacologically evoked activity in neural populations of restrained flies [23], detect mitochondrial Ca^{2+} in the muscles of behaving mice [24], and image the bioluminescent signals from individual neurons in disassociated cell cultures and *in vitro* preparations [16,25]. Here we describe the implementation of a novel technique that fundamentally extends these initial studies: a non-imaging setup for long term monitoring of GA bioluminescence that can report the activity of a small number of genetically specified neurons in the larval zebrafish during natural, unrestrained behavior. Although initially limited to behaviors occurring in darkness, we also describe and implement a novel bioluminescence detection strategy that uses stroboscopic illumination to reproduce natural lighting, and thus further extend this technique to the investigation of visually-driven behaviors.

Results

Neuroluminescence reports neural activity in behaving fish

The mechanism of Ca^{2+}-dependent bioluminescence from GFP-Aequorin (GA) and the steps to use GA as a neural activity reporter are schematized in **Supplementary Fig. 1**. Neuron-specific expression of GFP-apoAequorin (Ga), (**Supplementary Fig. 2**) was achieved by injecting single-cell embryos with plasmid encoding Ga downstream of the neuro-β-tubulin promoter (Nβt). High resolution 2-photon imaging also revealed the absence of any nonspecific expression in muscle (**Supplementary Fig. 3**) and variegated

expression levels in different brain regions (**Supplementary Fig. 4**). Following a 24 hour exposure to coelenterazine (CLZN), transgenic Nβt:GA zebrafish (**Fig. 1a**) were placed into the recording device (**Fig. 1b**) where they swam freely within a behavior chamber positioned directly beneath a large-area photomultiplier tube (PMT). While the PMT detected single photons emitted within the arena, an infrared CCD camera simultaneously tracked fish movement. Most bouts of spontaneous swimming coincided with the emission of large flashes of green light (**Fig. 1c–g**, **Supplementary Movie 1**), which occasionally were also observed without concurrent locomotion (**Fig. 1d**, arrowhead). The absence of any signal in Ga animals, untreated with CLZN, as well as in wild-type fish (with or without CLZN treatment) demonstrated that neuroluminescence required both the expression of Ga as well as exposure to CLZN (**Supplementary Fig. 5a**). Previous studies used alcohol as a solvent for CLZN reconstitution solutions [26], but we found that dissolving CLZN in 2-hydroxypropyl-β-cyclodextrin (CLZN-CDX) [27] also allowed, and possibly facilitated, *in vivo* formation of GA (**Supplementary Fig. 5b**) and avoided the negative effects of exposure to ethanol or methanol . Fish tested in cyclodextrin solution at a tenfold higher concentration then normally required showed no detectable changes in health or behavior (**Supplementary Fig. 5d**). With periodic replacement of the CLZN-CDX bath starting at 3 days-post-fertilization (dpf), large neuroluminescence signals were detected until at least 11 dpf, the last day tested (**Supplementary Fig. 5c**). Differences in neuroluminescence signal amplitude between individual larvae (**Supplementary Fig. 6a–c**) were apparent, possibly due to differential CLZN loading (**Supplementary Fig. 6d**,**e**) and animals that showed little or no responses were not tested further. Also, signal amplitude was found to depend on the type of CLZN used for GA constitution. Analogs of native CLZN have been developed that confer different binding affinities for calcium resulting in a range of sensitivities for the indicator [21]. We found that coelenterazine-*h* (CLZN-*h*) consistently produced better results than the native version and was therefore used in our experiments.

Neuroluminescence signals were large (signal to noise ratio >> 100), stable for long periods of time (>24 hours) (**Fig. 2a**), and coincident with spontaneous and evoked swim events (**Fig. 1c, Fig. 2**). Spontaneous signals detected from individual zebrafish spanned a range of sizes (**Fig. 2b**,**c**), exhibiting a smooth amplitude distribution with a high frequency of small events phasing into a long tail of increasingly large and rare events (**Fig. 2d**). After aligning individual signals to the initial onset inflection we estimate a time-to-peak of 5-10 ms and a slower decay time of ~ 25 ms (**Fig. 2c**), consistent with expectations for Aequorin and comparable to popular synthetic Ca^{2+}-indicators [21].

To measure neuroluminescence signals produced during stimulus-evoked behaviors, we delivered a mechanical tap below the swim chamber to elicit a startle response . Repeatedly evoked neuroluminescence signals were fast and consistently similar in amplitude (**Fig. 2e**). In order to isolate the sensory component of this response we then paralyzed the fish via a bolus injection of α-Bungarotoxin and repeated the experiment in the same animals (**Fig. 2f**). Figure 3g shows the aligned evoked signals from freely swimming fish in blue and from the same but paralyzed fish in red. The reduction in signal size following paralysis is not surprising; restrained fish show a substantial reduction spontaneous activity, possibly reflecting s state of behavioral suppression that effects both spontaneous and evoked behaviors (**Supplementary Figure 7**). Furthermore, we find very weak Ga expression levels in the trigeminal ganglion, one of the primary somatosensory ganglia known to mediate the tap-evoked escape response (**Supplementary Figure 4**), which can serve as an additional explanation for the reduction of the isolated sensory response in paralyzed fish.

To further investigate the origins of neuroluminescence, we exposed zebrafish to pentylenetetrazole (PTZ, 10 mM), an inhibitor of GABA-A receptors that induces epileptic-like neuronal discharges in humans, rodents and zebrafish [28]. Approximately thirty seconds after bath application of PTZ, zebrafish exhibited sustained periods of uncoordinated swimming accompanied by very large waves of neuroluminescence (**Fig. 2h, Supplementary Movie 2**). These early episodes (~3-5 min) were followed by

periodic bouts of clonus-like convulsions and prolonged waves of neuroluminescence that extended beyond the swimming bouts. (**Fig. 2i, Supplementary Movie 3**). PTZ evoked neuroluminescence signals of similar size and shape can also be detected in fully paralyzed fish (**Fig. 2j, Supplementary Movie 4)** and serve as a clear example of bioluminescence evoked in the absence of any motor activity.

Imaging the PTZ induced fluorescence changes of a large brain region in a transgenic fish expressing GCaMP2[29] under the HUC[30] promoter with two-photon microscopy uncovers long slow waves of correlated neural activity **(Supplementary Figure 8)** that are comparable with the neuroluminescence shown in Figure 3 h. These imaging experiments highlight the similarity of the bioluminescence signals to those obtained with conventional techniques.

Together, these results obtained with Nβt:GA indicate that neuroluminescence allows the non-invasive and long-term recording of population activity from freely behaving zebrafish larvae.

Neuroluminescence from genetically-targeted neurons

The hypocretin/orexin (HCRT) system in the hypothalamus consists of a group of neurons that is distinct, small in number (~ 20) and sits at the ventral limit of the diencephalon. It has been implicated in the control of arousal in mammals and fish [31-33] and its disruption in dogs and mice [34-35] produces symptoms similar to those of human narcolepsy, a disorder characterized by the sudden, spontaneous onset of sleep. Electrical recordings from HCRT neurons in rodents have found that these cells are active during periods of wakefulness and exhibit transient bouts of activity during phasic REM sleep [36-37]. In addition, specific optical stimulation of channelrhodopsin-2 expressing HCRT neurons in mice increased the probability of awakening from slow-wave sleep [38]. Over-expression of HCRT in zebrafish larvae promotes and consolidates wakefulness, induces hyperarousal and inhibits rest [32]. However, it has not been determined whether the activity of HCRT neurons in zebrafish is associated with periods of heightened activity, as has

been observed in mammals. To directly measure the activity of HCRT neurons during rest and wakefulness, we expressed Ga under the control of a HCRT promoter (**Fig. 3**) and monitored neuroluminescence throughout a circadian period. To record from this group of neurons is a significant test of the sensitivity of the neuroluminescence approach, because there are less than 20 HCRT neurons within ~100,000 neurons of the larval zebrafish nervous system. In addition, their location deep below the dorsal surface (>300 μm) results in considerable light scattering. Zebrafish larvae expressing Ga in HCRT neurons were treated with CLZN-*h* at 3 dpf and neuroluminescence was measured on subsequent days. With exposure to a natural light-dark cycle, zebrafish maintain a circadian periodicity in their rate of spontaneous swimming under constant lighting conditions. In the constant darkness of the neuroluminescence assay, larvae were found to increase their rate of swim bouts each morning, shortly after the time of normal lights-ON in the fish rearing facility (**Fig. 2a, 4a**). During these morning-active periods, as well as other periods of increased swimming activity [32], we observed an increase in the frequency of neuroluminescent signals from HCRT neurons (**Fig. 4a**). This is consistent with recordings from HCRT neurons in mammals [36]. Furthermore, when compared to Nβt:GA larvae (**Fig. 2a**), less neuroluminescence was detected in HCRT:GA fish when they were at rest or during brief arousals during the night (**Fig. 4a**). This suggests that HCRT neurons are specifically active during periods of consolidated locomotor activity and is in agreement with the hypothesis that HCRT promotes wakefulness and inhibits rest in zebrafish larvae [32], as in mammals [38].

To determine whether any proportion of the signals in HCRT:GA larvae were due to non-specific background effects, we used an imaging approach to localize the origin of the luminescence. Using an intensified-CCD camera in a custom-built bioluminescence/fluorescence microscope (**Fig. 5a**), we imaged restrained zebrafish and compared the spatial location of neuroluminescence to the location of GA expression as reported by the fluorescence of the tethered GFP (**Fig. 5b**). Again, bath application of PTZ

was used to induce epileptic events. As demonstrated in the whole brain two-photon imaging experiments (**SupplementaryFig. 8**), PTZ exposure induces strong and unspecific activity in most, if not all neurons across the brain, thus highlighting the usefulness of this treatment for control-experiments that test for the contribution of non-specific background expression to the neuroluminescent signals.

Although the zebrafish were paralyzed, this pharmacological stimulation produced transient increases in the total luminescence, similar to those detected in the non-imaging assay (**Fig. 5c**). During these transient neuroluminescence signals, ~90% of the emitted photons came from a region containing the HCRT somata (**Fig. 5d**, **e**). Photons originating from elsewhere within the fish head or tail were largely explained by the background dark-count rate generated by the detector. In addition, the small increase observed with respect to background might result from neuroluminescence generated in the processes of the HCRT neurons, which extend caudally into the spinal cord (**Fig. 3**). Similar experiments in restrained, but non-paralyzed, Nβt:GA and HCRT:GA fish confirm the absence of any detectable bioluminescence from muscle or other non-neuronal tissues (**Supplementary Fig. 9, 10 and 11**). Having confirmed the spatial origin of the neuroluminescence produced by HCRT:GA zebrafish, we next examined the properties of individual signals and their association with zebrafish behavior.

Individual neuroluminescence signals produced by HCRT neurons fell into two distinct amplitude categories (**Fig. 4b**). The aligned signals from individual zebrafish were easily classified into large or small signals with a manually determined threshold of peak amplitude (**Fig. 4c**). This bi-modal amplitude distribution differed from the continuous distribution measured for Nβt:GA neuroluminescence events (**Fig. 4d**). Both large and small signals were associated with swim bouts, but the latency of a behavioral response and the distance swum following either signal amplitude consistently differed (**Fig. 4e**). Signals classified as small HCRT events were followed by a short latency behavior. In contrast, behaviors following large HCRT events occurred 15-30 ms later. Accurate estimation of the neuroluminescence-to-behavior

latency was accomplished by fitting the raw photon signal with a dual-exponential function, determining the peak-time, and measuring the time from the peak until the subsequent behaviors exceeded a velocity threshold (**Fig. 4f**). The histograms of response latencies for large and small HCRT signals are distinct and the average latencies are significantly different ($p < 0.001$; Student's T-test: n = 359 small events, n = 135 large events from 5 fish). Furthermore, small HCRT signals were more likely to be preceded by a behavioral response than large HCRT signals. These preceding behavior events result in latency estimates less than zero. Excluding events of clearly inverted causality, (latencies of less than -50ms, 47 of 359 small events versus only 1 of 135 large events) the average response latencies for both amplitude classes of HCRT signals were significantly longer than the latencies observed for Nβt:GA neuroluminescence signals (**Fig. 4g**), suggesting that swim bouts associated with HCRT events represent a distinct subset of the spontaneous behaviors produced by larval zebrafish (5 HCRT fish, small events (S): 17.6 +/– 1.0 ms, n = 312, large events (L): 40.8 +/– 1.6 ms, n = 134; 6 NβT fish: 11.3 +/– 0.4 ms, n = 1667 – S versus PN: $p < 0.001$, L versus PN: $p < 0.001$). Further analysis of the behaviors associated with the different amplitude HCRT signals (**Supplementary Figure 12**) revealed that the peak velocity following the small events significantly exceeds that of large events. This analysis also revealed that large events are preceded by increased swim activity compared to small events in a one second time window preceding the HCRT event.

These results highlight that neuroluminescence signals have sufficient temporal resolution to compare neurophysiological and behavioral responses on a time scale of ~10 ms in addition to the capability of distinguishing between responses that differ in amplitude. Whether the small and large HCRT signals result from activating different subsets of the labeled neurons or whether the different amplitudes originate from distinct activation states of the entire population is unknown. We also cannot completely rule out that the small events originate from some unspecific background expression since the control PTZ

experiments described in Figure 6 might lack the necessary sensitivity to pick out these relatively small signals.

To explore the limits of neuroluminescence sensitivity, we investigated whether our technique can detect signals from a single HCRT neuron (**Supplementary Fig. 13**). For this we expressed transiently Ga in HCRT neurons and screened for fish that showed expression in only a single cell (**Supplementary Fig. 13a**). After treatment with CLZN-*h* and exposure to PTZ we observed neuroluminescent signals that were small but still well above the detection limit (**Supplementary Fig. 13b**), a clear demonstration that neuroluminescence can be detected from single neurons.

Monitoring neuroluminescence during visual behavior

Using existing detection methods, bioluminescence experiments have been limited to behaviors that occur naturally in darkness. Imperfections in spectral filters, particularly their inability to adequately reject the high-angle (>30°) light incident on the detector, have necessitated that the photon-counting sensor be protected from all but infrared illumination, to which most sensors are largely insensitive. To overcome this problem, we have designed a novel detection system that uses a cathode-gated channel photon multiplier (CPM) with a temporal gating strategy that allows fast flickering visible illumination during the detection of the bioluminescence signal.

In our design, computer generated gating signals control the cathode-voltage of the CPM, a visible LED, and the IR illumination light source for a behavior monitoring camera. During each 10 ms cycle, the CPM is gated “ON” for 9 ms, and is able to detect individual bioluminescence photons. In the final 1 ms, the CPM is rapidly gated “OFF” and both the visible LED and IR illumination are briefly activated, sending ~10^{12} visible photons towards the now insensitive detector for 1 ms. In the next cycle, the CPM is again gated “ON” and able to count single bioluminescent photons. With this 100 Hz repetition rate and a 90% detection

duty cycle, natural illumination conditions can be simulated while only 1 of 10 emitted bioluminescent photons is discarded (**Fig. 6a**).

We have tested our time-gated detection/illumination strategy by exposing groups of Nβt:GA zebrafish to short visible light cycles (5 min ON, 5 min OFF). Zebrafish respond to transient decreases in illumination with an increase in swim activity, while an elevation in light levels is followed by a period of suppressed activity (**Fig. 6b**, **c**). These transient behavioral responses to changes in light intensity are in line with previously reported observations [32]. We were able to record this visually-driven behavior while simultaneously recording neuroluminescence signals, demonstrating that the neuroluminescence assay can be extended to experiments requiring natural lighting conditions.

Discussion

Our results demonstrate a novel technique for monitoring neural activity in freely behaving animals. We show that Ca^{2+}-dependent bioluminescence can be detected from a small number of genetically specified neurons, even just a single cell, and that this signal can be monitored continuously for days while an animal freely behaves within an illuminated environment. This technique offers great potential for future investigations of the neural control of behavior in zebrafish and other neuroscience model systems.

The future development of modified forms of Aequorin, akin to the significant enhancement of other genetically encoded calcium indicators [39], as well as the use of existing or novel CLZN analogs [21] that confer increased Ca^{2+} sensitivity to Aequorin will further extend the sensitivity of the neuroluminescence technique. Indeed, recent advances in optimizing emission properties of different bioluminescent probes have facilitated their use at the single cell level [16,22] and manipulated their calcium sensitivity [40]. Furthermore, the development of new light detectors with improved quantum efficiency for both non-imaging assays (e.g. with large-area avalanche photodiodes and gallium-arsenide-phosphate PMTs) and

photon-counting imaging setups (e.g. with electron multiplying CCDs) [41] offer exciting future possibilities for improving GA signal detection.

However, it is likely that the current version of GA, as is the case for existing fluorescent genetically-encoded Ca^{2+} indicators, lacks the sensitivity to detect individual action potentials [42]. We thus expect that the neuroluminescence responses detected with our system primarily result from bursts of firing rather than from individual action potentials. With existing versions of Aequorin, bioluminescence signals evoked by as little as five action potentials have been detected from individual pyramidal neurons in brain slices [42] and these signals showed relatively linear characteristics at higher stimulus intensities. This indicates that our technique is comparable in its sensitivity to existing genetically encoded calcium indicators [43]. However, in order to relate neuroluminescence signals quantitatively to the underlying number of action potentials, it is necessary to conduct careful electrophysiological studies separately in each model system and, ideally, in each neuronal sub-population. Nonetheless, these preliminary results suggest that, while individual action potentials are likely to remain undetected, bursts of a few spikes should result in identifiable bioluminescent signals. An indicator that reliably reports bursts of activity is unquestionably useful, especially if it can be targeted to specified subclasses of neurons that are hypothesized to be involved in a natural behavior. In addition, we are highly encouraged by the quantitative properties of neuroluminescence demonstrated by the results with HCRT:GA zebrafish (**Fig. 4 b–g**). Not only are we able to isolate two distinct event amplitudes in a freely swimming zebrafish, but the two amplitude classes were reliable predictors of distinct behaviors. As this technique is applied to different populations of neurons, we expect not only to gain insights about the timing of activity in such a population in the context of natural behaviors, but also to get a reliable report of the magnitude of these activations - another valuable source of information to assist in decoding how the neurons of the brain control an animal's behavior.

We anticipate the use of expression targeting strategies, including cell-type specific promoters and binary expression systems such as UAS/Gal4 [44] to target GA to a wide variety of brain regions and specific neural populations. For example, available promoters for the serotonergic dorsal *raphe nuclei* [45] or the dopaminergic system [46] can be used to investigate the role of these neurotransmitters and the associated cell populations in various behavioral contexts. With the continued development of behavioral assays and techniques for stimulating and ablating neurons [10,47-48], neuroluminescence has the potential to provide an essential tool for determining how the brain choreographs the complex behavioral patterns of a simple vertebrate.

In addition to the larval zebrafish, neuroluminescence detection during free behavior could be applied to other popular neuroscience model systems. For example, the fruit fly *Drosophila melanogaster* has been used successfully in bioluminescent imaging assays to study circadian clock genes [49] and to image neural activity in restrained fruit flies [23]. Similarly, using a neuroluminescence strategy in the small and genetically accessible *Drosophila* larvae or the nematode *C. elegans* should facilitate the long-term and cell-specific recording of neural activity in any behavioral assay. In mammals, the bulk neuroluminescence from genetically distinct neuron types could be recorded during natural behavior with chronically implanted optical fibers [50].

We believe that the fast, stable properties of GA's report of neural activity along with non-imaging detection strategies provide a useful, easily implemented tool for monitoring the activity of genetically specified cell types during natural behavior; an attractive alternative to more technically challenging imaging approaches currently being pursued.

Acknowledgments

We thank W. Hastings and T. Wilson for bountiful advice, discussion, and generously providing an intensified CCD camera. We also thank L. Tricoire for the kind gift of the GA construct; M. Orger, A. Douglass, P. Ramdya, and members of the Engert and Schier labs for comments and advice; A. Douglass for *Nβt:gal4* vectors; P. Ramdya for providing the *nacre* strains; and B. Obama for his stimulation package. We thank Steven Zimmerman, Karen Hurley, and Jessica Miller for excellent zebrafish care. This work was funded by the McKnight Foundation (F.E.), the Harvard Mind, Brain, and Behavior post-doctoral fellows program (A.R.K.), and the NIH (A.F.S., D.P.).

Author contributions

E. A. N. and A. R. K. designed the assay and performed the experiments. E. A. N., A. R. K., and F.E. analyzed the data. D. A. P. and A. F. S. generated the HCRT:Ga transgenic line and assisted with behavioral analysis. E. A. N., A. R. K., D. A. P., A. F. S. and F.E. prepared the manuscript. E. A. N. suffered the most.

Materials and Methods

Zebrafish

Zebrafish (*Danio rerio*) of the *mitfa*$^{-/-}$ (*nacre*) strain were used in all studies; they lack body pigmentation and are therefore significantly more translucent than wild type strains. Zebrafish were maintained on a 14/10 hr light-dark cycle and fertilized eggs were collected and raised at 28°C. Embryos were kept in E3 solution (5 mM NaCl, 0.17 KCl, 0.33mM CaCl2, 0.33 mM MgSO4). All experiments were approved by Harvard University's Standing Committee on the Use of Animals in Research and Training.

Vector construction and transgenic lines

The coding sequence of GFP Aequorin, GA5v1 (a gift from L. Tricoire), referred to throughout the text as Ga, was subcloned via PCR into a neuro-β-tubulin expression vector (Nβt*:GFP*) (a gift from Paul Krieg) into an AgeI and NotI site, resulting in *tol2:Nβt:Ga:tol2*. *UAS:Ga* was constructed by subcloning the coding sequence after the *UAS:E1B* sequence in the *UAS:Dsred Express-1* expression vector by replacing DsRed by blunt end insertion at the AgeI/Not I site. To express Ga in HCRT neurons, the zebrafish HCRT promoter, containing 1 kb of genomic DNA immediately upstream of the HCRT start codon, was subcloned upstream of Ga to yield *tol2:HCRT:Ga:tol2*. Plasmid DNA (20ng/µl in 100 mM KCl) was injected into *nacre* zebrafish embryos at the single cell stage for transient expression. To generate stable transgenic zebrafish, *tol2:Nβt:Ga:tol2* or *tol2:HCRT:Ga:tol2* was co-injected with *tol2* transposase mRNA. Injected embryos were grown in E3 solution and screened for expression at 2-5 dpf, and positive individuals (F0) were grown to adulthood and out-crossed to *nacre* zebrafish. F1 progeny of this cross were screened for expression at 2-5dpf, and transgenic founders with the best expression levels were identified. Most experiments with *Nβt:Ga* transgenic zebrafish were performed with progeny (F3) of crosses of stable F2 transgenics

(heterozygous) and wild-type nacre zebrafish . Hypocretin experiments were performed by crossing *HCRT:Ga* F0 founders to wild-type nacre zebrafish .

Aequorin reconstitution

Zebrafish larva were raised in E3 medium and screened for GFP fluorescence of Ga at 3 dpf. For reconstitution with coelenterazine (CLZN), 5-10 larvae were transferred into 2 ml of E3 solution containing a final concentration of 40 µM CLZN-*h* (Biotium, USA) or *native* CLZN (Invitrogen, USA or Biotium, USA) (all stock solutions at 10 mM dissolved in 45% 2-hydroxypropyl-b-cyclodextrin (Invitrogen, USA) were kept at -80°C to minimize auto-oxidation). After 24-48 hours, larvae were washed repeatedly in E3 medium and maintained in new E3 medium until they were transferred to the recording chamber (0-3 hours). In some experiments fish were transferred back into freshly prepared E3-CLZN solution after a neuroluminescence recording session and washing was repeated before the next set of experiments.

Bioluminescence detection and behavior monitoring

Within a light-proof enclosure, the bioluminescence and behavior setup (**Fig. 1b**) was assembled and aligned using structural framing (80/20, USA) and optomechanic components (Thorlabs, USA). Zebrafish were placed in ~1 ml of E3 solution contained in a circular behavior chamber machined from clear-acrylic (12.5 mm in diameter and 6.25 mm in depth) enclosed on the top and bottom with cover glass. To avoid bubble formation in long term or overnight recordings, silicone sealant was used to keep the cover glass held in position. The chamber was mounted as close as physically possible (~5 mm) to a large-area photon-counting PMT (H7360-02: Hamamatsu, Japan) with USB interface counting unit (C8855: Hamamatsu, Japan), thus maximizing the angle of light collected by the detector (>60°). An 880 nm infrared LED ring light (Advanced Illumination, USA) was placed above the recording chamber, surrounding the PMT. The low-incident angle of the LEDs allowed the zebrafish to be illuminated while only minimally

directing light into the PMT. To further limit bleed through of the IR illumination light into the sensitive detector, a 700nm short-pass filter (Chroma, USA) was placed at the entrance to the PMT. An infrared-sensitive CCD camera (C4900, Hamamatsu, Japan) was positioned beneath the behavior chamber and imaged the zebrafish behavior via a close-focus manual zoom lens (58-240: Edmund Optics, USA). The camera's sensitivity allowed for low-light IR illumination, but was limited to 30 Hz frame acquisition rates. However, software de-interlacing and cropping of the video signal resulted in 60 Hz frame rates (frame period of 16.67 ms) at 250x240 pixels.

Depending on the experiment, single fish or groups of up to 10 were included in the chamber. In some experiments, PTZ was added to induce epileptic events, while keeping the final volume constant. To evoke escape responses, zebrafish were stimulated with a mechanical tap delivered to the behavior chamber by a custom-designed computer controlled electromagnetic lever. Photon count data from the PMT, behavior image data from the CCD, and experiment/stimulus control was accomplished with a custom multi-threaded C++ program. However, Labview drivers (National Instruments, USA) are available for the USB counter and the camera frame-grabber (PCI-1407, National Instruments, USA). To minimize the amount of behavioral data recorded, images were compressed with a custom compression algorithm that stored only pixels with intensity changes larger than the camera noise threshold and permitted continuous behavior monitoring for days. In some *HCRT:GA* experiments, IR illumination was strobed for 20 ms at 1 Hz and camera frames were synchronously acquired at 1 Hz, thus minimizing bleed-through into the PMT but allowing the classification of behavior into active and inactive seconds based upon whether the fish had moved since the last frame acquisition. All data analysis was performed with custom Matlab software (Mathworks, USA). Individual bioluminescent events were fitted with a double exponential function:

$$y(t) = 2 * A \frac{e^{\frac{O-t}{\tau_2}}}{1 + e^{\frac{O-t}{\tau_1}}}$$

where τ_1 is the time constant for the rising phase, τ_2 the time constant for the decay and A and O fit the Amplitude and the horizontal offset respectively.

In-vivo two-photon imaging of GA expression, coelenterazine loading and HUC: GCaMP2 fluorescence

Prior to imaging, larvae were anaesthetized using 0.02% Tricaine (Sigma, USA) in E3 and embedded in low melting point agarose (1.2% w/v). Tricaine was removed and α-Bungarotoxin (1 mg/ml, Sigma, USA) was injected into the ventral region of the spinal cord using a pulled glass pipette, inducing paralysis and preventing movement artifacts. Expression profiles or coelenterazine loadings were imaged at high resolution with a custom built two-photon microscope[10] employing a Ti:Sapphire laser (Spectra Physics, USA) tuned to 920 nm for Ga and 850 nm for CLZN. All data acquisition and analysis was performed using custom Labview (National Instruments, USA), Matlab (Mathworks, USA) and C++ software.

Single photon imaging

Using a modified commercial imaging system (Xenogen, USA), a custom designed microscope was built to allow magnification of the zebrafish brain onto an image intensifier, which amplifies light via an electron multiplication stage that is directed onto a phosphor screen that is imaged by a conventional CCD camera. The microscope incorporated an Blue-UV LED illuminated epifluorescence pathway for imaging GA expression prior to photon counting and a 20X water immersion objective with a 0.95 numerical aperture (Olympus, Japan). A manual z-stage allowed adjustment of the focal plane within the zebrafish brain (Newport, USA). A USB frame-grabber (Sensoray, USA) was used to acquire raw images from the

CCD, and custom C++ and Matlab (Mathworks, USA) software was used to detect single photon positions and exclude cosmic rays. After being treated with CLZN-*h* and washed with E3, zebrafish were prepared as described above for two-photon imaging. After acquiring a fluorescent image by exciting GA positive neurons with UV light and a bright field image to localize the GA positive neurons within the fish, baseline photon emission was recorded. To identify the neuronal source of any emitted photons, PTZ (10 mM) was used to maximally excite all neurons in the fish. Recordings were made continuously for approximately an hour. Analysis of the photon source position was performed by examining periods of transient increases in full field photon emission similar to those detected in the free-behavior assay. All analysis was performed with custom Matlab software.

Bioluminescence detection during natural lighting

Within a light-proof enclosure, the bioluminescence and behavior setups were assembled as described above. The following differences were implemented: A channel photon multiplier CPM (MP 1984 CPM, Perkin Elmer Optoelectronics, Germany) with a 520/60 nm band-pass filter (Chroma, USA) was mounted directly above the recording chamber. A yellow LED (peak emission: 587 nm, luminous intensity: 1900 mcd, RadioShack, USA) was directed towards the behavior chamber from the side. A high-speed, infrared-sensitive CCD camera (Pike, Allied Vision Technology, USA) was installed beneath the behavior chamber. An Infrared filter (Hoya filter, R72, B and H Photo, USA) was mounted on the camera lens to prevent bleed through of the visible illumination light into the camera. The camera's sensitivity allowed for low-light IR illumination with frame rates exceeding 100 Hz.

During bioluminescence measurements, groups of up to 10 NβT GA fish were placed into the chamber. Computer generated timing signals (C++ and Labview, National Instruments, USA) controlled the IR illumination of the infrared LED ring light, the stimulus LED, and the camera exposure times. During one

illumination cycle, the CPM was initially gated on for 9 ms and sensitive to individual bioluminescent photons after which it was rapidly gated OFF for 1 ms. While the CPM was off, the IR illumination and visible LED were briefly switched on for 0.8 ms and a camera exposure was acquired. This recording-illumination cycle was repeated at 100 Hz, producing the illusion of constant visible illumination while still allowing 90% of the emitted bioluminescence photons to be detected by the CPM.

Figure Legends

Figure 1 – Monitoring the neural activity of freely behaving zebrafish

a Dorsal (left) and lateral (right) fluorescence/bright-field micrographs of a 7 dpf *Nβt:Ga* transgenic zebrafish larva (scale bar: 0.20 mm). **b** Neuroluminescence setup: A large-area (25 mm diameter) photon-counting PMT is situated above a transparent behavior chamber (12.5 mm diameter). The highly-sensitive light detector is protected by an infrared (IR)-blocking filter such that a ring of 880 nm light-emitting diodes can be used to illuminate the behavioral chamber. Fish are imaged with an IR-sensitive CCD camera positioned below the chamber. The large spectral separation between GA bioluminescence and the IR illumination allows the simultaneous recording of neuroluminescence signals and the behavior of freely swimming zebrafish larvae. **c** Exemplary neuroluminescence recording of a 7 dpf *Nβt:Ga* transgenic zebrafish larva previously exposed to coelenterazine. Photon emission and behavior (swim speed in millimeter moved per frame period (mm/16.67 ms)) are shown for a 30 second recording. A mechanical stimulus was delivered at 15 s (*), inducing a fast startle response and a large increase in neuroluminescence. **d** An expanded view of the boxed region indicated in **c** highlights a neuroluminescence event not associated with locomotion (arrowhead). **e** Raw image acquired by the IR CCD camera during neuroluminescence recording (scale bar: 1.5 mm). **f** Superposition (inverted grayscale) of all frames acquired during the 30 second recording period shown in **c**, the entire fish trajectory is shown. **g** The fish trajectory shown in **f** is overlaid with a colored line for which the neuroluminescence amplitude at each segment is coded as the line-width, (*) indicates the time of the mechanical stimulus.

Figure 2 – Neuroluminescence and behavior of NβT GA zebrafish

a Neuroluminescence signals and behavior can be monitored continuously for several days; a 16 hour excerpt of the recording from a 6 dpf *Nβt:Ga* transgenic zebrafish, following 24 hours of exposure to coelenterazine, is shown. Despite the constant dark conditions of the assay, an increase in locomotor activity, measured as the number of active seconds in a ten minute sliding window (bold line), and a corresponding increase in neuroluminescent events occurs soon after the previously experienced light-on time (9 AM) of the zebrafish light-dark rearing cycle. This is expected from a circadian modulation of spontaneous swimming . **b** Expanding the bracketed region indicated in **a** reveals the range of neuroluminescence signal amplitudes that occur during spontaneous behavior. **c** Upon aligning all the signals detected during the 16 hour recording to each signals onset time and color coding each event by the number of photons arriving in a 50 ms window (0 to >2,000, see color bar), we find that neuroluminescence events consist of a fast rise and slower decay in light emission with a large range of peak amplitudes. **d** The histogram of signal amplitudes observed from NβT GA zebrafish (n = 6 fish, 3,125 events), normalized to the maximum signal detected from each individual, demonstrates the frequent occurrence of small amplitude events and a long tail of the distribution populated by increasingly large and rare events. **e** A mechanical stimulus was delivered to a group of freely swimming zebrafish (n = 6) by tapping the recording chamber (stimulus times indicated by the star symbol (*)). The stimulus resulted in neuroluminescence signals coincident with the evoked startle responses, surrounded by intermittent and variable spontaneous signals. **f** The same fish shown in **e** were paralyzed with α-Bungarotoxin and received the same mechanical stimulus (*). Paralysis permitted isolating the sensory component of the neuroluminescence event from the full escape response behavior elicited in freely-swimming animals. **g** The aligned stimulus-driven events in each condition are compared, revealing an attenuated but clearly detectable sensory signal in paralyzed zebrafish. **h** PTZ induced epileptic behavior, characterized by

uncoordinated rapid swimming, is associated with large, fast bursts of neuroluminescence consistent with the strong neural activation expected during seizure episodes (t_0 = 1 min after initial PTZ exposure). **i** Following extended exposure to PTZ (t_0 > 17 min), long, slow neuroluminescence events are observed independent of swimming. **j** Paralyzed zebrafish exposed to PTZ also exhibit long, slow neuroluminescence events, suggesting that motor activity may modulate the amplitude and timescale of PTZ induced epileptic episodes.

Figure 3 – Targeted Ga expression in Hypocretin neurons

a Expression of Ga in the ~20 Hypocretin (HCRT) neurons of a transgenic 4 dpf zebrafish larva are imaged with a wide-field fluorescence microscope, demonstrating their position within the posterior diencephalon (scale bar: 100 µm). **b** Ga-expressing HCRT neurons shown in a maximum intensity projection of image sections acquired with a two-photon microscope (imaged region indicated by red rectangle in **a**); note the long, dorsal-caudal projecting axons with an expansive arborization near the zebrafish otic vesicle (scale bar: 50 µm) .

Figure 4 – Activity in Hypocretin neurons during natural behavior

a A freely behaving 4 dpf zebrafish larva exhibits periods of increased spontaneous locomotor activity. The longest active period occurs soon after the light-on time (9 AM) of the normal rearing light cycle. Neuroluminescence events primarily occur during these periods of heightened activity. **b** Expanding the bracketed region indicated in **a** reveals that these neural signals fall into two distinct amplitude classes. Manually determined thresholds (200 photons/50 ms in **b**) were used to classify individual events into a large and small amplitude group. **c** The amplitude classified signals from the entire recording of the larva shown in **a** are aligned and the thick lines indicate the average signal time course within each class. **d** Histogram of the amplitudes for all HCRT neuroluminescence events (n = 1,064, 8 fish), normalized to the maximum response within each fish, are compared to the response amplitude of NβT:GA fish (NβT) shown in **Figure 2d**. Signals classified as large and small are colored accordingly and are clearly distinct. **e** The mean distance swum, aligned to the position of the fish at the time of a HCRT signal (0 ms), is plotted for the frames immediately before and after HCRT signals of each amplitude class (error-bars represent s.e.m.). Notably, fish swim sooner and further following small HCRT events than following large HCRT events. **f** A double exponential fit of neuroluminescence signals was used to identify the peak of the event. Example fits (solid curves) are shown for events (open circles) from the two amplitude classes along with the corresponding swim-velocities. Latency was measured as the time from the peak of the response to time at which the zebrafish achieved a threshold swim velocity (0.25 mm/16 ms). **g** Histograms of event-to-behavior latencies for the large and small HCRT events as well as events analyzed for NβT:GA zebrafish (NβT); the distributions are distinct.

Figure 5 – Bioluminescent photons are generated by the GA-targeted HCRT neurons

a Schematic diagram of photon-counting imaging apparatus: an intensified CCD camera, custom epi-fluorescence microscope, and excitation light (UV LED) are assembled within a light tight enclosure. **b** The rectangle overlay indicates the region imaged to localize Aequorin expression via GFP fluorescence in a HCRT-GA larva immobilized in low melting point agarose and paralyzed with α-Bungarotoxin. The arrow indicates the HCRT somata (scale bar: 100 μm). **c** When epileptic-like neural activity is induced by the addition of PTZ (10 mM), transient increases in the total number of photons arriving throughout the entire image field were observed (brackets). **d** The positional origin of the detected photons during these transient events is plotted. The majority of photons arrive from the region containing the HCRT neurons; the spread is likely caused by scattering in the biological tissue while the homogenous background signal results from dark counts at the detector (scale bar: 100 μm, arrow shown at same position as **b**). **e** The photon flux arriving from within four regions of interest (see inset): the HCRT somata, the imaged portion of the zebrafish head excluding the HCRT somata, the rostral tail, and the background. The number of photons arriving from non-HCRT region of the zebrafish head is only slightly above the background dark counts and may represent photons originating from the axonal processes of the HCRT neurons (see **Figure 3**) (error bars represent s.e.m.). However, after adjusting for the dark count signal, we still observe that >90% of photons arrive from the region containing the HCRT somata.

Figure 6 – Temporally gated detection for monitoring neuroluminescence during visual stimulation

a Schematic of timing protocol for stroboscopic visual stimulation and gating of a Channel Photon Multiplier (CPM) during a "light ON" to "light OFF" transition. Close-ups of the 100 ms surrounding the transition and 10 ms of a "light ON" gate cycle demonstrate the synchronous control of the bioluminescence detection and behavior monitoring. When visual stimulation is required, the visible LED is switched on for 0.8 ms while the CPM is off gated. **b** Example of neuroluminescence and visually-evoked behavior recorded during periodic changes in whole-field illumination. 6 dpf Nβt:GA transgenic zebrafish larvae, previously exposed to CLZN, show reduced locomotor activity and Nβt:GA neuroluminescence signal during "light ON" periods. **c** The mean neuroluminescence and behavioral response surrounding an step increase in whole-field illumination (63 light transitions, 7 experiments, 49 fish).

Supplementary Figure 1 – Neuroluminescence in zebrafish: mechanism and method

The upper diagram (**a**) schematizes the molecular reaction underlying the Ca^{2+}-dependent light emission of GFP-Aequorin (GA) and the lower diagram (**b**) demonstrates how GA was employed as a bioluminescence reporter of neural activity in freely swimming zebrafish. **a** Light emission first requires the reaction of GFP-apoAequorin (Ga) with coelenterazine. After reacting with oxygen to form a stable peroxide intermediate, a coelenterazine molecule will stably bind to Ga to form GA. In this reconstituted form, the binding of Ca^{2+} ions induces a conformational change in GA that initiates the oxidative decarboxylation of coelenterazine, releasing CO_2 and producing an excited enolate anion. By a process known as non radiative chemiluminescent resonance energy transfer (CRET), the energy from the excited anion is transferred to GFP and results in the emission of a green photon. After photon emission, both the coelenteramide and Ca^{2+} are released and Ga is again available for reconstitution. **b** Neural expression of Ga is achieved by microinjecting embryos at the single-cell stage with plasmid DNA encoding Ga under control of a neuron specific promoter. Generation of stable transgenic fish or other expression targeting methods (e.g. electroporation) can also be used to introduce Ga into neurons of interest. Neuronal Ga is exposed to coelenterazine *in* vivo, in order to form the luminescent GA, by immersing the entire zebrafish larva in embryo medium containing coelenterazine dissolved in cyclodextrin. After an incubation time, neural Ca^{2+}-dependent light emission, neuroluminescence, can be detected during unrestrained behavior.

Supplementary Figure 2 – Neural specific expression of GFP-Aequorin (Ga)

a Bright field and fluorescence micrographs of a 7 dpf transgenic NβT:Ga larval zebrafish (scale bar: 0.2 mm). **b** A two-photon optical section through the dorsal midbrain and hindbrain (scale bar: 100 μm). **c-d** Two-photon maximum intensity z-projections of the left optic tectum in two zebrafish larvae that transiently expressed Ga following plasmid injection at the single-cell stage. The *neural-β-tubulin* promoter specifically targets Ga expression to neurons, which appear healthy during all observed developmental stages (3-10 dpf) (scale bar: 20 μm).**c** Mosaic expression of Ga with *neural-β-tubulin:Ga* (6 dpf).**d** Expression of Ga by co-injection of plasmids encoding *neural-β-tubulin:Gal4* and *UAS:Ga,* demonstrating that a binary expression system can be used to target Ga expression to specific neurons (6 dpf).

Supplementary Figure 3 – Neural specific expression of GFP-Aequorin (Ga) in the Zebrafish Tail

a (left) Dorsal bright field micrograph of a 7 dpf zebrafish (scale bar: 0.3 mm). (middle) An expanded view of the region indicated (red rectangle) focusing on the tail of the fish. Neurons of the spinal cord (*) are located along the midline above the notochord. Axial musculature surrounds the fish tail. Epaxial muscles are not easily visible on the dorsal side, but the lateral hypaxial muscles (M), and the segregated myotomes, are clearly visible (scale bar: 50 μm). (right) A higher magnification image of the indicated region (blue rectangle) reveals the dark stripes characteristic of the sarcomeres of skeletal muscles (M) (scale bar: 20 μm). **b** (left) Dorsal bright field and fluorescence micrograph of a 7 dpf transgenic Nβt:Ga zebrafish (scale bar: 0.3 mm). The indicated region (red rectangle) shows the position of subsequent two-photon investigation of Ga expression. (middle) A maximum intensity projection of a series of images acquired with a two-photon microscope through the complete depth, 370 μm, of the tail (scale bar: 50 μm). Specific neural expression in spinal cord neurons and lateral axon tracks (*) can be seen in the center; a few neural processes and auto-fluorescence from skin is detected in the region overlapping with the lateral hypaxial muscles (M). (right) A zoom-in on the indicated region (blue rectangle) further demonstrates that Ga expression is only detected in neuronal structures (scale bar: 20 μm). **c** (left) Lateral bright field micrograph of a 7 dpf zebrafish (scale bar: 0.3 mm). (middle) An expanded view of the region indicated (red rectangle) focusing on the tail of the fish. Neurons (*) of the spinal cord are positioned dorsal to the notochord. The segregated myotomes of the axial musculature that surrounds the fish (M) can be seen (scale bar: 50 μm). (right) A higher magnification of the indicated region (blue rectangle) also reveals dark stripes characteristic of the sarcomeres of skeletal muscles (M) and the location of the spinal cord track(*) (scale bar: 20 μm). **d** (left) Lateral bright field and fluorescence micrograph of a 7 dpf transgenic Nβt:Ga zebrafish (scale bar: 0.3 mm). The indicated region (red rectangle) shows the position of subsequent two-photon investigation of Ga expression. (middle) A maximum intensity projection of a series of images acquired with a two-photon microscope through the complete depth, 250 μm, of the tail (scale bar: 50 μm).

Specific neural expression in spinal cord is apparent; only neural processes and auto-fluorescence from skin is observed in the region overlapping with the axial muscles (M). (right) A zoom-in on the indicated region (blue rectangle) further demonstrates that Ga expression is only detected in neuronal structures (scale bar: 20 μm). Arrows indicate neural processes innervating the musculature.

Supplementary Figure 4 – Neural specific expression of GFP-Aequorin (Ga) in Trigeminal Neurons

a (left) Dorsal bright field and fluorescence micrographs of a 7 dpf transgenic Nβt:Ga zebrafish (scale bar: 0.3 mm). Rectangle indicates the region imaged with two-photon microscopy. (middle) A maximum intensity projection through the ventral portion of the left optic tectum (OT) and trigeminal nucleus (scale bar: 50 μm). (right) A higher magnification image of the indicated region (blue rectangle) reveals the low expression level of Ga in trigeminal neurons (arrow) compared to other neurons of the zebrafish brain (scale bar: 20 μm). **b** (left) Lateral bright field and fluorescence micrographs of a 7 dpf transgenic Nβt:Ga zebrafish (scale bar: 0.3 mm). Rectangle indicates the region imaged with two-photon microscopy. (middle) A maximum intensity projection of sagittal sections through the right optic tectum (OT) and trigeminal nucleus (scale bar: 50 μm). (right) A higher magnification image of the indicated region (blue rectangle) again reveals the low expression level of Ga in trigeminal neurons (arrow) compared to the more dorsal neurons of the zebrafish brain (scale bar: 20 μm). Note that only neural structures are visible, even though expression level varies, and that there is no detectable expression in regions where facial and axial muscles are located.

Supplementary Figure 5 – Reconstitution of Aequorin with coelenterazine

a Total light emission produced by groups of five 5-6 dpf larvae representing different Ga and coelenterazine (CLZN) combinations. Neuroluminescence is only detected from Ga transgenic zebrafish after soaking in embryo medium containing 40 μM coelenterazine (Ga & CLZN), suggesting that detected photons were generated by reconstituted Aequorin. Ga transgenic zebrafish raised in normal embryo medium (Ga only), *nacre* wild-type zebrafish soaked in normal embryo medium (wildtype only) or *nacre* wild-type zebrafish soaked in embryo medium containing 40 μM coelenterazine (wildtype & CLZN) show no photon emission. The low number of photon events detected for the other conditions arise from dark counts generated at the PMT photocathode. The Y-axis for each experimental group is offset by 25 counts to facilitate comparison between the different conditions. **b** The average number of photons within the transient neuroluminescent events produced by GA in zebrafish exposed to CLZN dissolved in ethanol or cyclodextrin are shown. Fish were tested in groups of 5 (n = 30) for 10 minutes (error bars represent s.e.m.). **c** Cyclodextrin-dissolved coelenterazine is able to reconstitute Aequorin and sustain neuroluminescence until at least 11 dpf (a two minute recording from an 11 dpf GA zebrafish shown). The coelenterazine bath solution was replaced every 2 days. **d** Wild-type zebrafish were exposed to a ten-fold higher concentration (400 μM) of Cyclodextrin (CDX) without coelenterazine from 3 dpf to 5 dpf and tested for behavioral activity (the number of 10 ms periods in which motion was detected per second). When compared to untreated siblings (fish were tested in groups of 5 with a total of 80 fish in each condition), no difference in activity level was observed (error bars represent s.e.m.).

Supplementary Figure 6 – Variation in signal amplitude and coelenterazine loading

a-c Neuroluminescence signals produced by three 6 dpf zebrafish siblings and their corresponding swim velocity (mm/frame period (16.67 ms)). Each sibling was exposed to CLZN-*h* for 24 hours under identical conditions (in the same rearing dish). Neuroluminescence corresponding to behavioral events can be detected in all 3 individuals; however, the peak signal amplitudes vary from fish to fish. For the fish shown in **a**, small neuroluminescence events are visible, but almost no baseline neuroluminescence is detectable, whereas the fish in **b** and **c** show not only larger transient neuroluminescence signals, but also an increase in the baseline neuroluminescence which possibly reflects a corresponding increase in background neural activity. **d-e** Two-photon horizontal sections through the optic tectum and the otic vesicle comparing the amount of CLZN-fluorescence in 4 dpf non-transgenic *nacre* zebrafish (scale bar: 40 μm). A control zebrafish not exposed to CLZN exhibits strong auto-fluorescence from the skin, but weak auto-fluorescence within the brain. **e** Individual larvae exposed to CLZN 24 hours prior to imaging exhibit strong fluorescence in neural tissue resulting from the excitation of CLZN that was absorbed into the brain. Each image is color coded according to reflect the calibrated CLZN concentration (see gradient scale). Weak signal in cell body regions could be caused by exclusion of CLZN from the nucleus of neurons, however, CLZN is clearly detected within the brain of each larva and the observed differences in concentration may explain some of the observed variability in peak neuroluminescence signals.

Supplementary Figure 7 – Restraining zebrafish substantially reduces spontaneous activity

a A single image of a freely swimming zebrafish (top) and the minimum intensity projection of a 3 second image sequence (bottom) (scale bar: 2.5 mm). **b** The activity of a 6 dpf fish, measured as the frame to frame pixel change (acquired at 50 Hz) normalized to the maximum value, is plotted for a 60 second time period. Each peak in the activity recording, which corresponds to a discrete swim bout, is counted as a single motion event. **c** A single image of a partially restrained zebrafish (top), and a maximum intensity projection of a 3 second image sequence (bottom) during a bout of spontaneous behavior (scale bar: 0.35 mm). The fish's head is embedded in low melting agarose, but the tail is free to move. **d** The activity of a head-restrained 6 dpf fish, measured as the frame to frame pixel change (acquired at 50 Hz) normalized to the maximum value, is plotted for a 60 second time period. Each peak in the activity recording, which corresponds to a discrete bout of tail motion, is counted as a single motion event. Note that a complete lack of activity in the restrained fish is interrupted by a brief burst of struggle-like bouts of tail motion. **e** A comparison of the mean number of spontaneous motion events per minute in free versus head-restrained zebrafish reveals a dramatic reduction in spontaneous activity during restraint (n = 10 zebrafish in each group, 5-6 dpf, error bars represent s.e.m.).

Supplementary Figure 8 – PTZ evoked calcium responses in HuC:GCaMP2 transgenic zebrafish

a (left) Dorsal bright field micrograph of a 7 dpf zebrafish (scale bar: 0.15 mm). The rectangle indicates the region selected for calcium imaging. (middle) A HuC:GCaMP2 zebrafish was embedded in low melting agarose, paralyzed, and imaged with a two-photon microscope. The average intensity image of the acquired time-series reveals expression of GCaMP2 in the optic tectum (OT), midbrain, and hindbrain of this transgenic zebrafish (scale bar: 50 μm). (right) Regions of interest within the right and left tectal neuropils, midbrain somatic region, and hindbrain are shown; these regions were used in analysis of the calcium-dependent fluorescence signal. **b** During PTZ exposure, sporadic waves of correlated activity were detected throughout the zebrafish brain. The integrated δF/F (%) signals from each region are shown in the corresponding color; a vertical line aligned to the earliest signal peak (in the tectal neuropil) is shown to facilitate comparison of the peak signal times in the different brain regions. These transient responses have time courses comparable to the sustained neuroluminescence events observed in paralyzed Nβt:GA zebrafish (**Figure 3j**). **c-d** An additional example of the experiment described in **a-b** in which a larger, more dorsal plane of the zebrafish brain was investigated. **c** (middle image, scale bar: 100 μm) **d** Unlike in **b**, the hindbrain is the final region to reach peak signal intensity.

Supplementary Figure 9 – Photons are generated by neural structures in Nβt:GA transgenic fish

a Schematic diagram of photon-counting imaging apparatus: an intensified CCD camera, custom epi-fluorescence microscope, and excitation light (UV LED) are assembled within a light tight enclosure. **b** A 5 dpf Nβt:GA larva was immobilized on its side in low melting point agarose and the rectangle overlay indicates the region imaged to localize Aequorin expression via GFP fluorescence. The arrow indicates the dorsal portion of the zebrafish brain and the auto-fluorescent swim bladder is indicated with a star symbol (*) (scale bar: 100 μm). **c** When epileptic-like neural activity is induced by the addition of PTZ (10 mM), transient increases in the total number of photons were observed . **d** The positional origin of the detected photons during these transient events is plotted. Also in a non-paralyzed zebrafish, the majority of photons arrive from the region containing neurons of the brain and spinal cord (CNS); arrow and start symbol (*) are located at the same position as in **b** (scale bar: 100 μm). **e** The photon flux (photons/pixel/second) from within three regions of interests (see inset): CNS, the imaged portion of the zebrafish excluding the CNS, and the background (error bars represent s.e.m.). Photon flux from the non-neuronal region of the zebrafish is slightly above the background dark counts, which could result from photons that originate from neurons being scattered by the fish body tissue or from neural processes located throughout the fish.

Supplementary Figure 10 – Photons are generated by neural structures in the spinal cord

a Schematic diagram of photon-counting imaging apparatus: an intensified CCD camera, custom epi-fluorescence microscope, and excitation light (UV LED) are assembled within a light tight enclosure. **b** A 5 dpf Nβt:GA larva was immobilized on its side in low melting point agarose and the rectangle overlay indicates the region imaged to localize Aequorin expression via GFP fluorescence. The arrows indicate regions of the spinal cord and the auto-fluorescent swim bladder is indicated with a star symbol (*) (scale bar: 100 μm). **c** When epileptic-like neural activity is induced by the addition of PTZ (10 mM), transient increases in the total number of photons were observed . **d** The positional origin of the detected photons during these transient events is plotted. The majority of photons arrive from the region containing neurons of the spinal cord; arrows and star symbol (*) are located at the same position as in **b**. **e** The photon flux (photons/pixel/second) from within three regions of interests (see inset): spinal cord, the imaged portion of the zebrafish excluding the spinal cord, and the background (error bars represent s.e.m.). Photon flux from the non-neuronal region of the zebrafish is slightly above the background dark counts, which could result from photons that originate from neurons being scattered by the fish body tissue or from neural processes located throughout the fish.

Supplementary Figure 11 – Photons are generated by GA-targeted HCRT neurons in restrained fish

a Schematic diagram of photon-counting imaging apparatus: an intensified CCD camera, custom epi-fluorescence microscope, and excitation light (UV LED) are assembled within a light tight enclosure. **b** A 5 dpf HCRT-GA larva was immobilized in low melting point agarose and the rectangle overlay indicates the region imaged to localize Aequorin expression via GFP fluorescence. The arrow indicates the HCRT somata (scale bar: 100 μm). **c** When epileptic-like neural activity is induced by the addition of PTZ (10 mM), transient increases in the total number of photons were observed . **d** The positional origin of the detected photons during these transient events is plotted. Also in a non-paralyzed zebrafish, the majority of photons arrive from the region containing the HCRT neurons; the arrow is located at the same position as in **b** (scale bar: 100 μm). **e** The photon flux (photons/pixel/second) from within four regions of interests (see inset): HCRT neurons, the imaged portion of the zebrafish head excluding the HCRT region, the rostral tail, and the background. Photon flux from the non-HCRT head region of the zebrafish is slightly above the background dark counts, which may represent photons originating from the axonal processes of the HCRT neurons (see **Figure 4**) or photons from HCRT neurons that are scattered within the fish body tissue.

Supplementary Figure 12 –

Different amplitude signals from HCRT neurons are correlated with different behaviors

a The mean velocity of freely swimming HCRT:GA zebrafish in the two second time period surrounding large and small HCRT events (event time = 0 ms).The thin lines surrounding each mean plot demarcate a boundary of +/–2 s.e.m. **b** An expansion of the time immediately surrounding the HCRT event. The difference in response latency for large and small HCRT events is apparent, as well as different velocity profiles (error bars represent s.e.m.). **c** Comparing the mean velocity within 1 second preceding the HCRT events (bracketed time region shown in **a**), demonstrates that zebrafish are more active prior to a large HCRT event than a small HCRT event. **d** Comparing the mean peak velocity reached following different HCRT events reveals that fish swim faster after a small HCRT event than after a large HCRT event (error bars represent s.e.m.).

Supplementary Figure 13 – Neuroluminescence detection from single HCRT neurons

a Fluorescence micrograph of a zebrafish larva transiently expressing HCRT: Ga in a single neuron (soma indicated by arrow, scale bar: 100 μm). **b** Following constitution with CLZN for 24 hours, epileptic-like neural activity was induced by the addition of PTZ (10 mM), and large neuroluminescence signals were easily detected from an individual neuron in a freely moving animal.

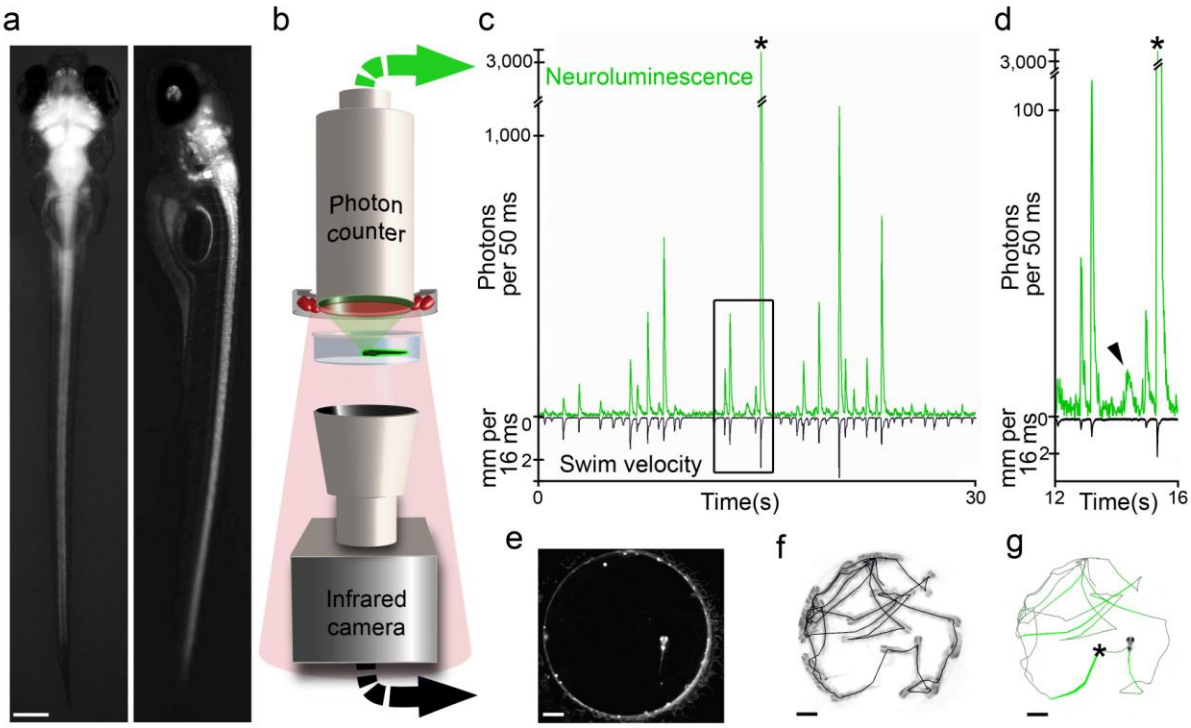

Engert_Figure1

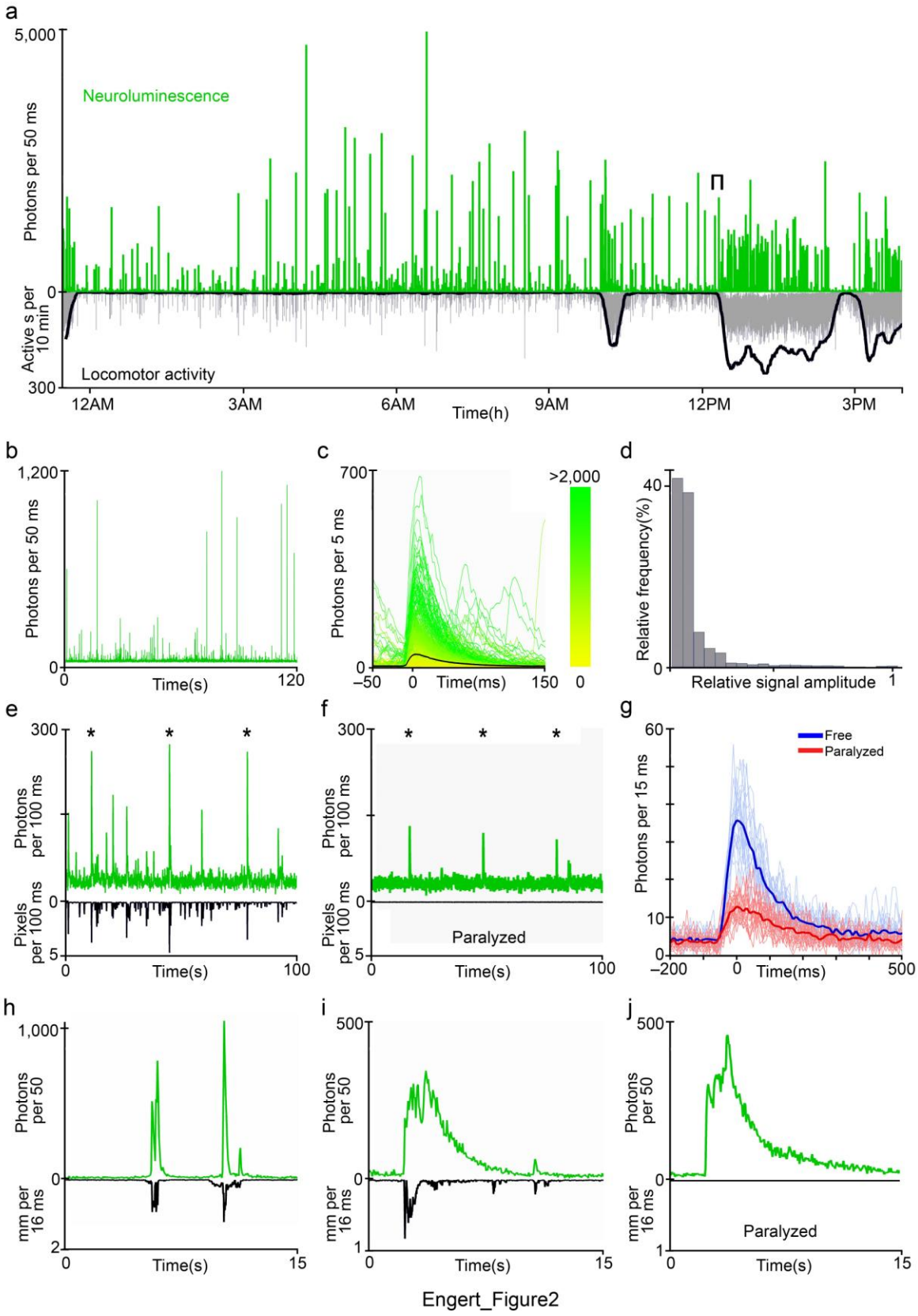

Engert_Figure2

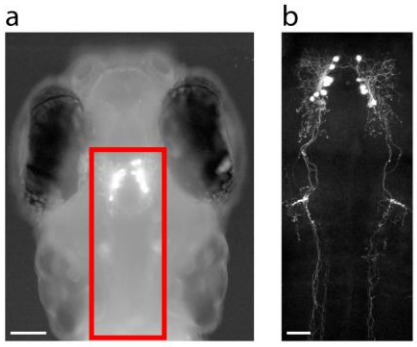

Engert_Figure3

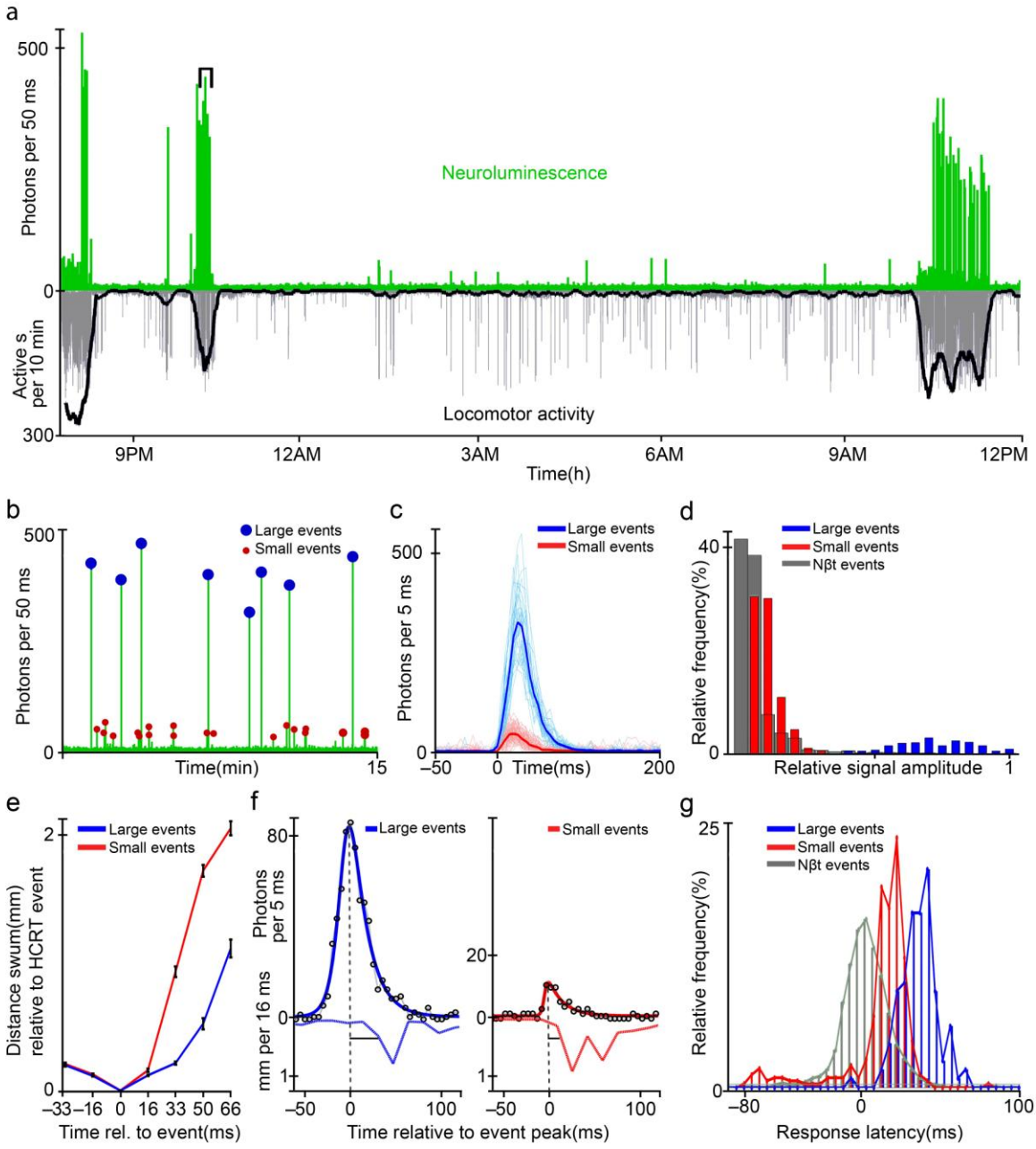

Engert_Figure4

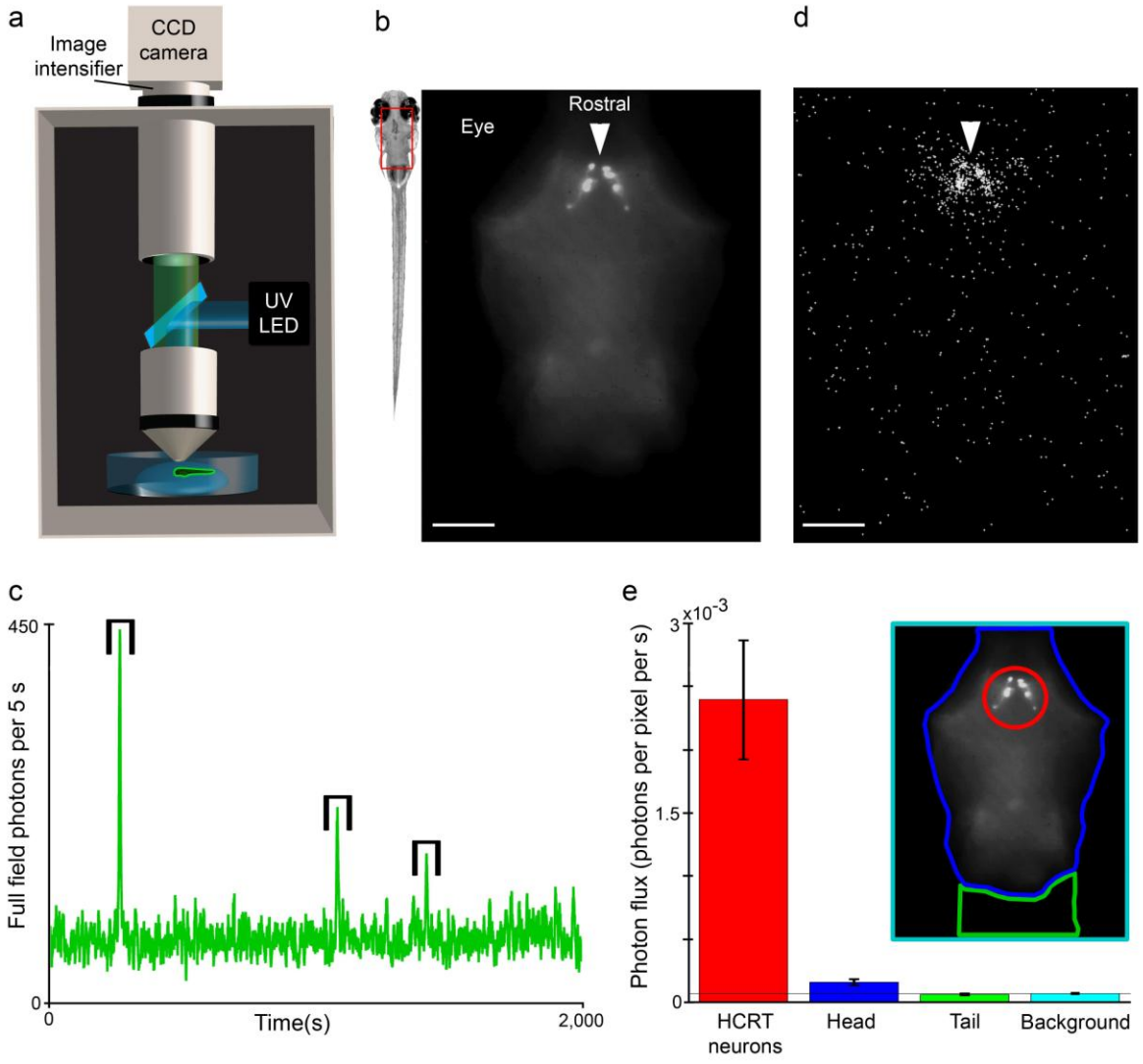

Engert_Figure5

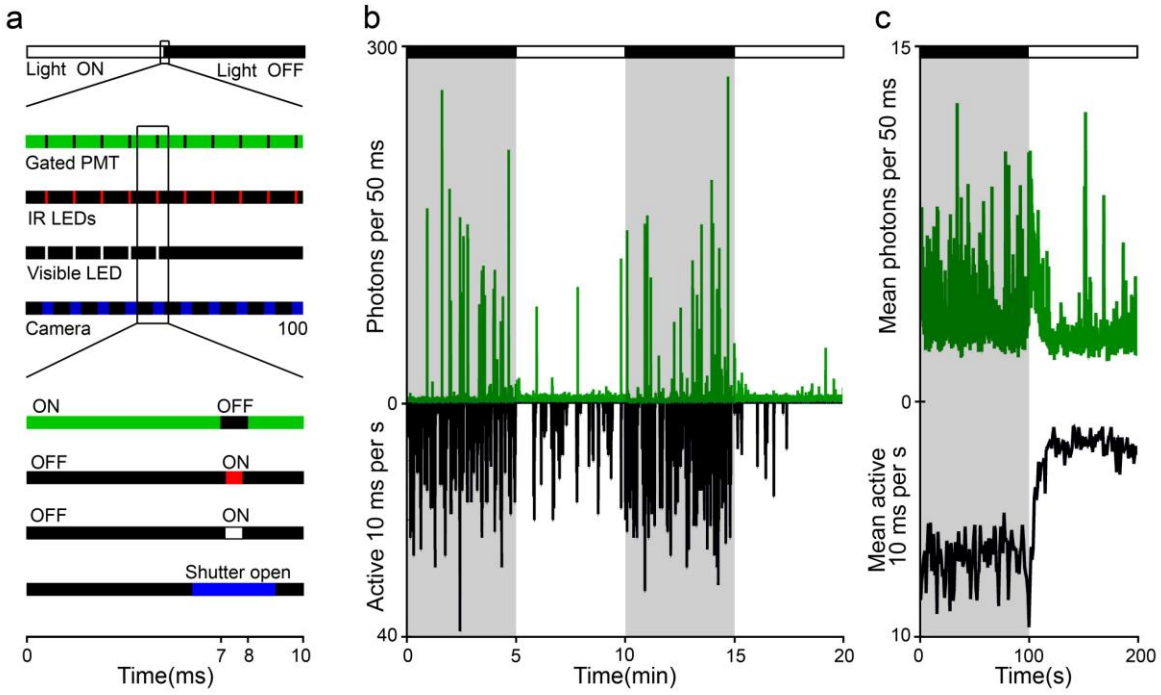

Engert_Figure6

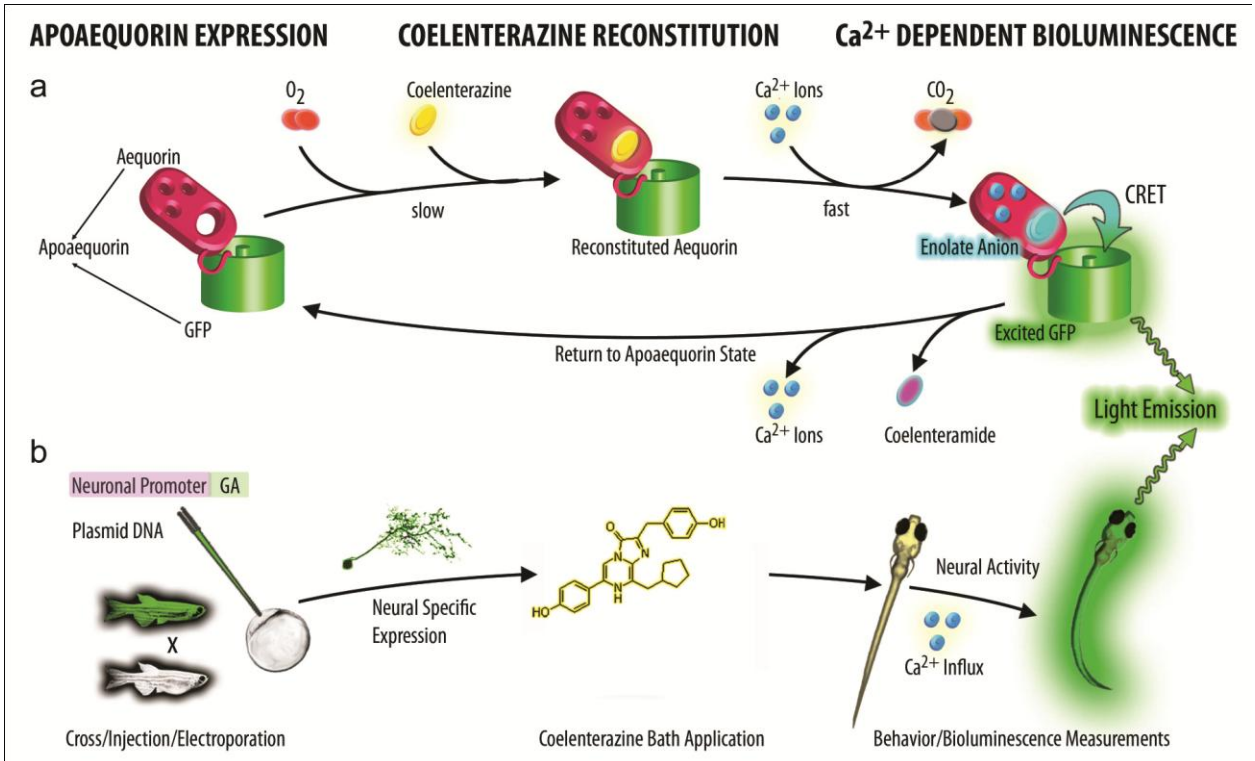

Engert_SupplementaryFigure1

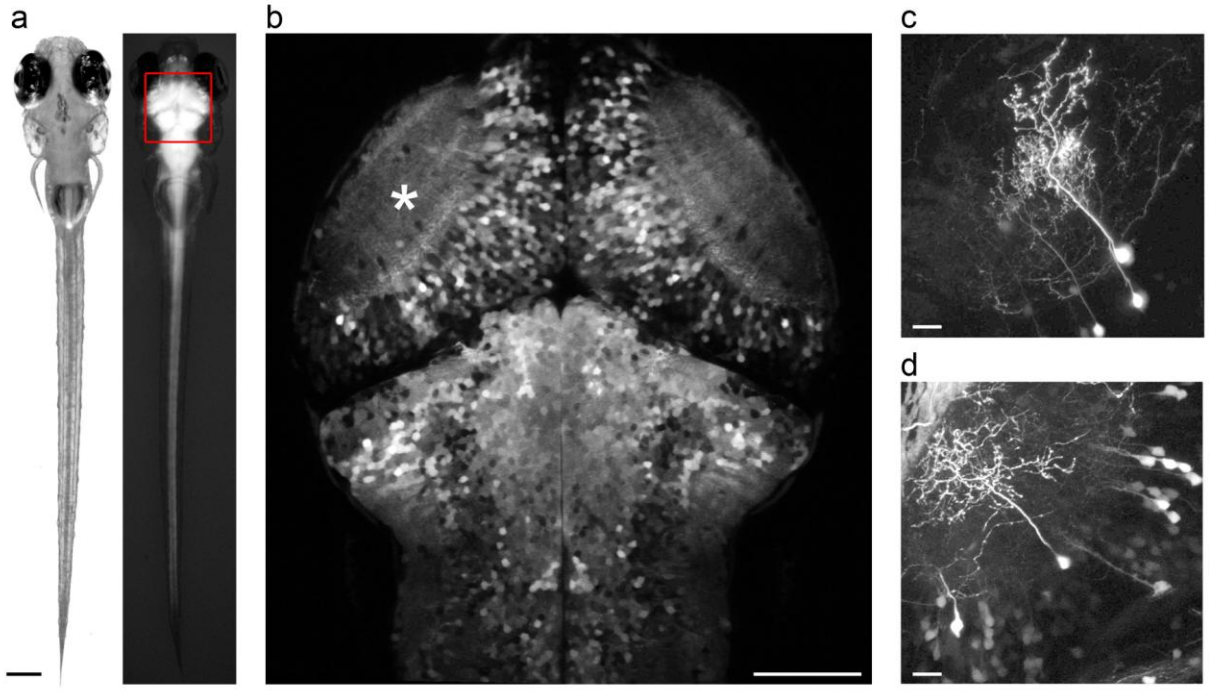

Engert_SupplementaryFigure2

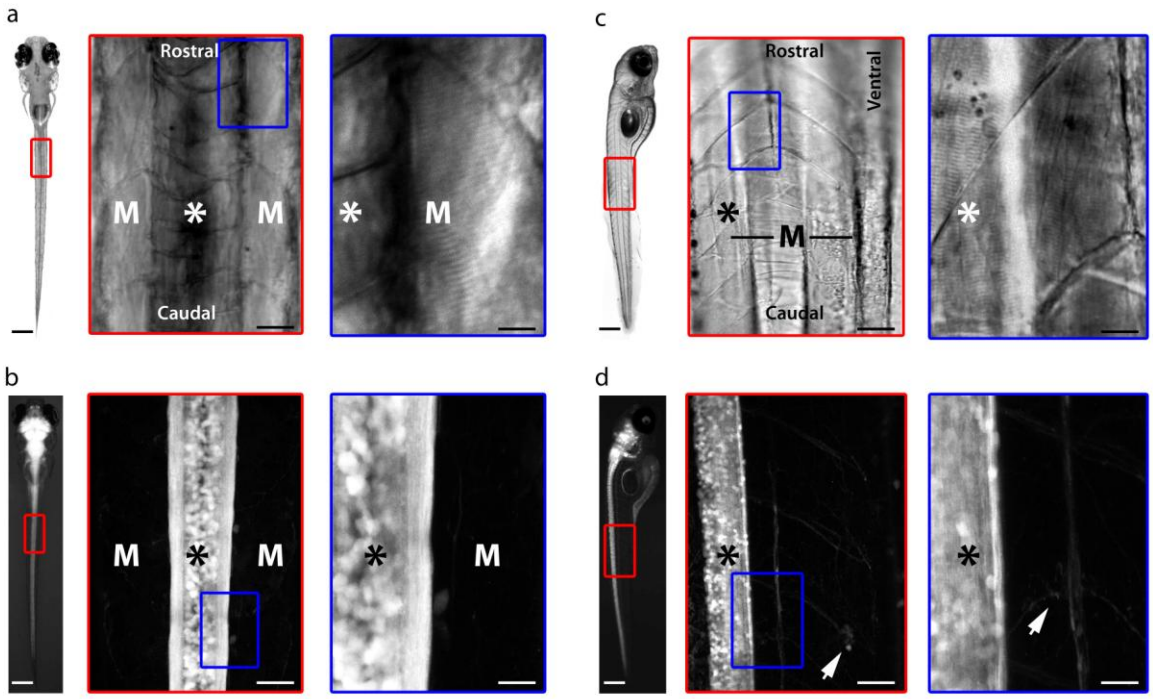

Engert_SupplementaryFigure3

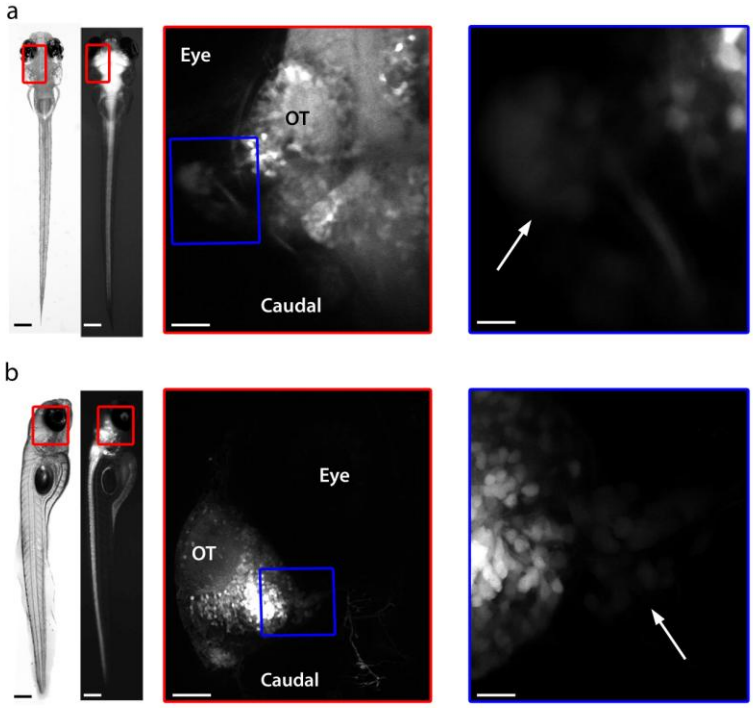

Engert_SupplementaryFigure4

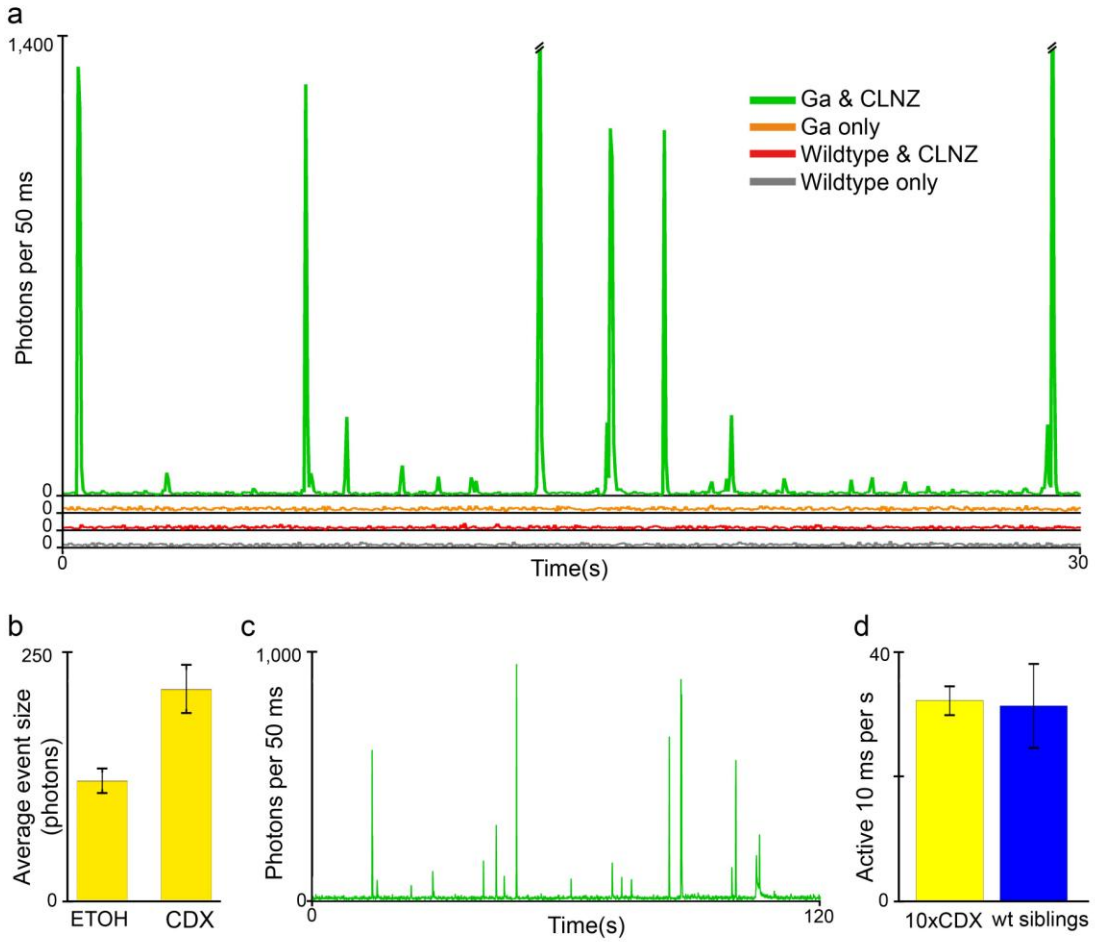

Engert_SupplementaryFigure5

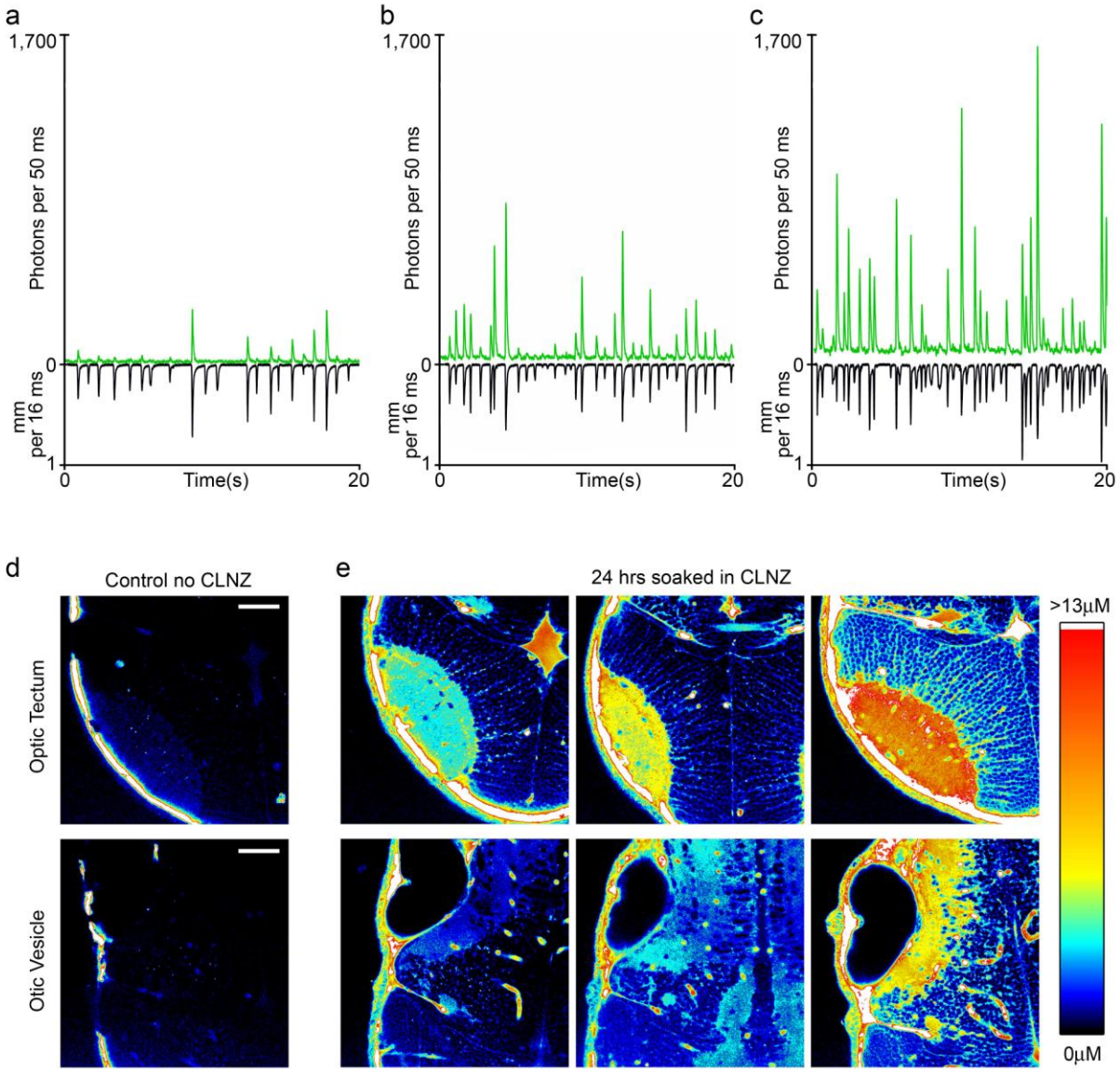

Engert_SupplementaryFigure6

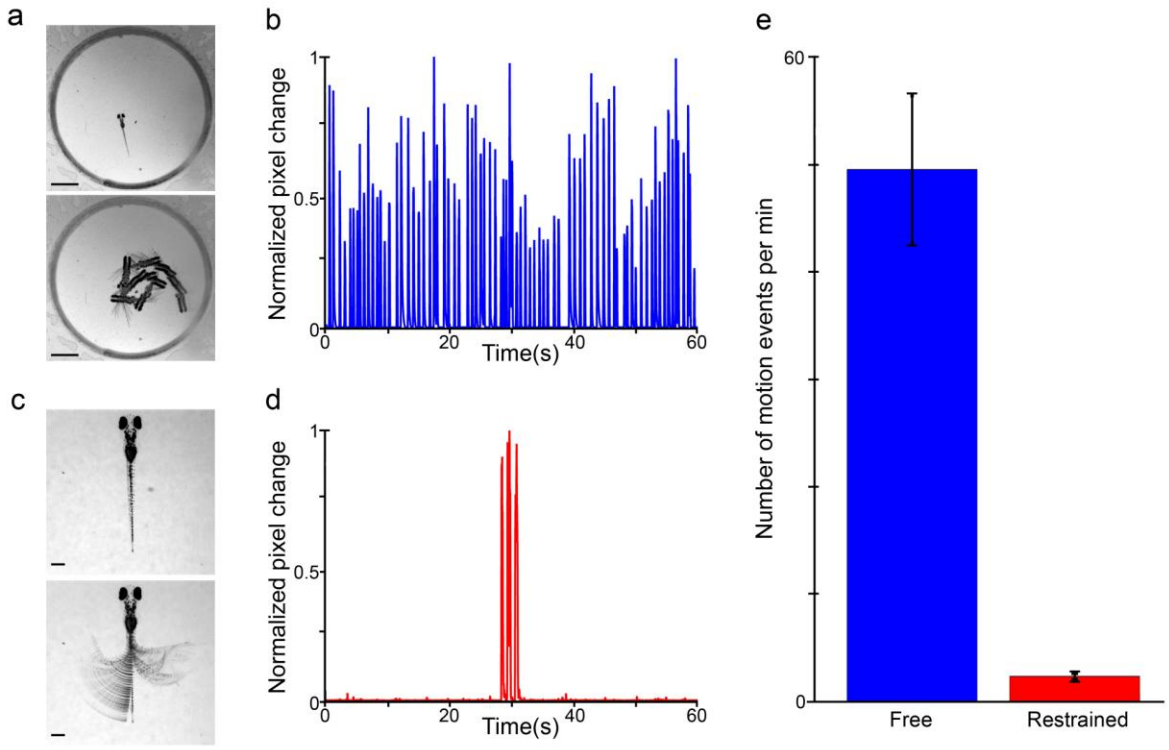

Engert_SupplementaryFigure7

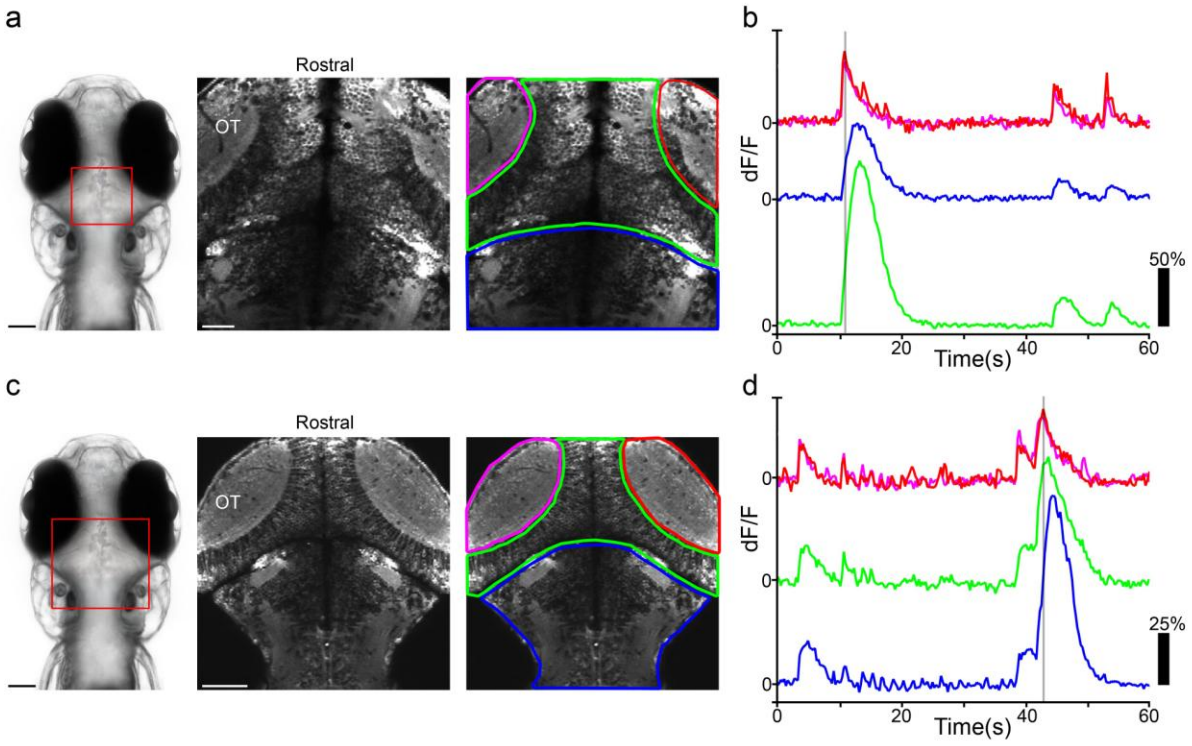

Engert_SupplementaryFigure8

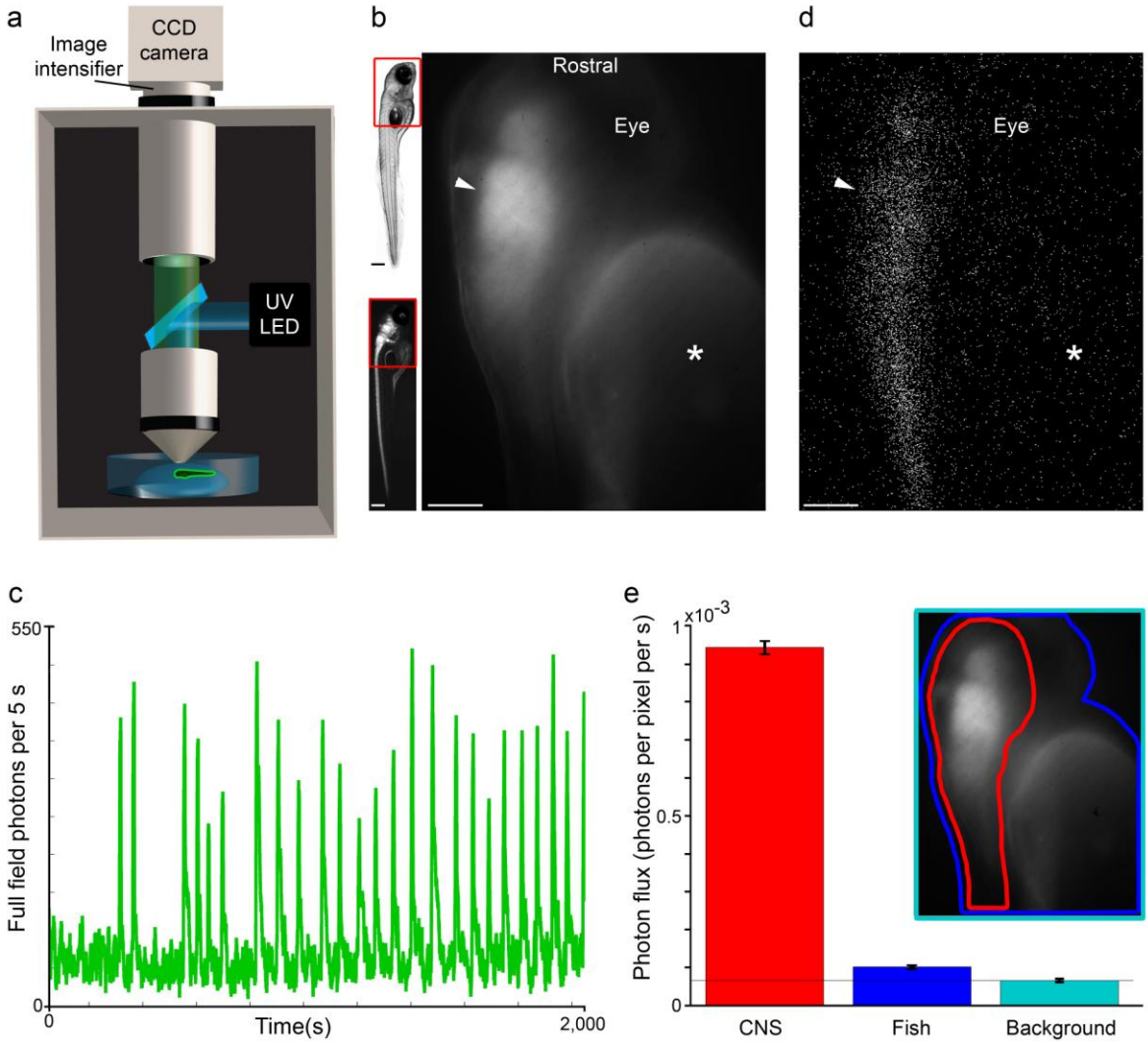

Engert_SupplementaryFigure9

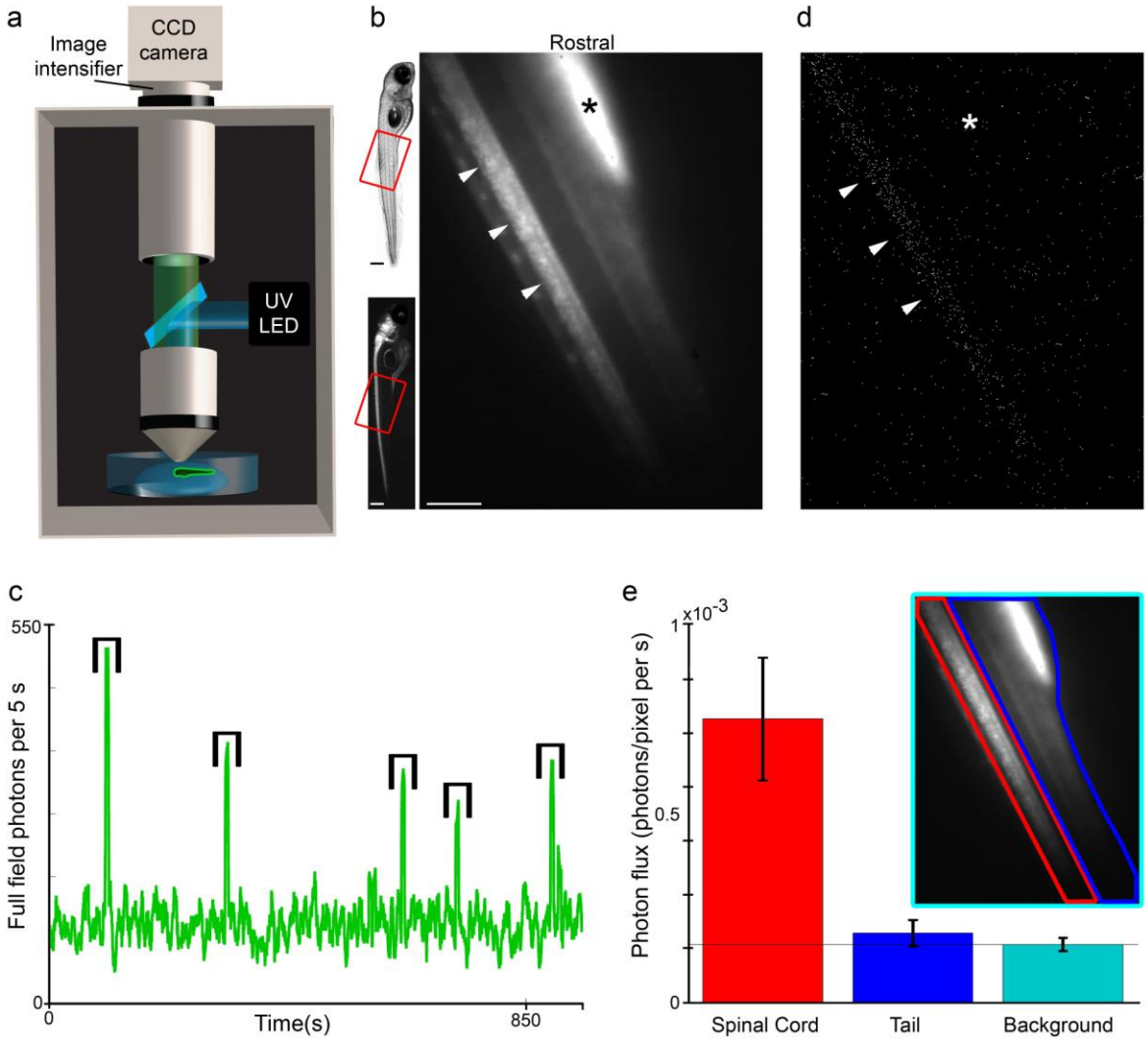

Engert_SupplementaryFigure10

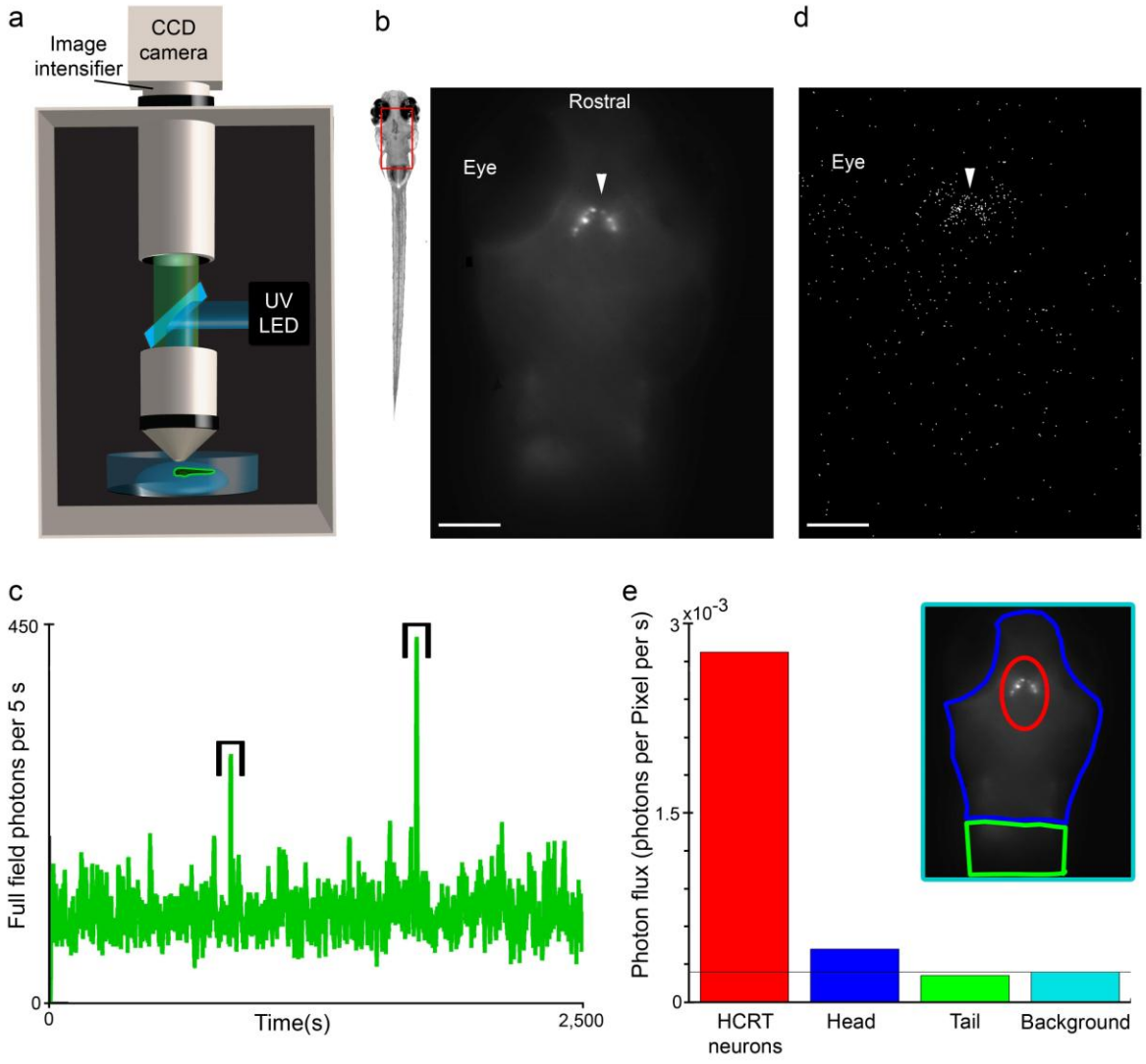

Engert_SupplementaryFigure11

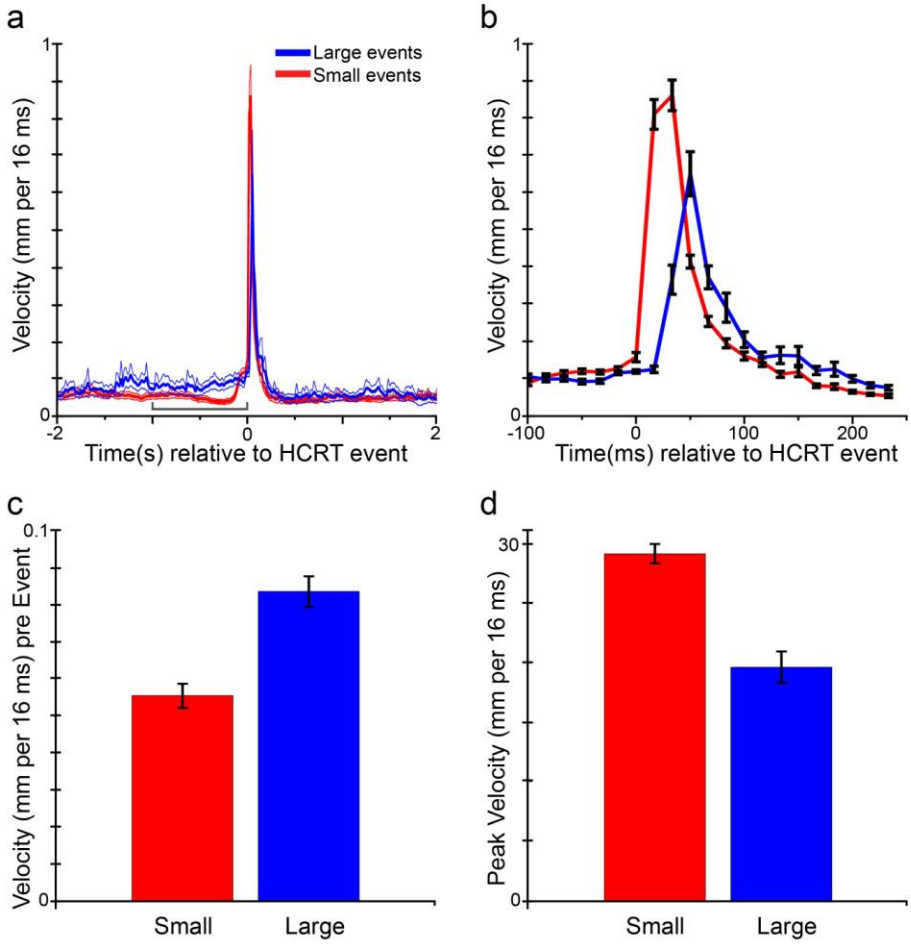

Engert_SupplementaryFigure12

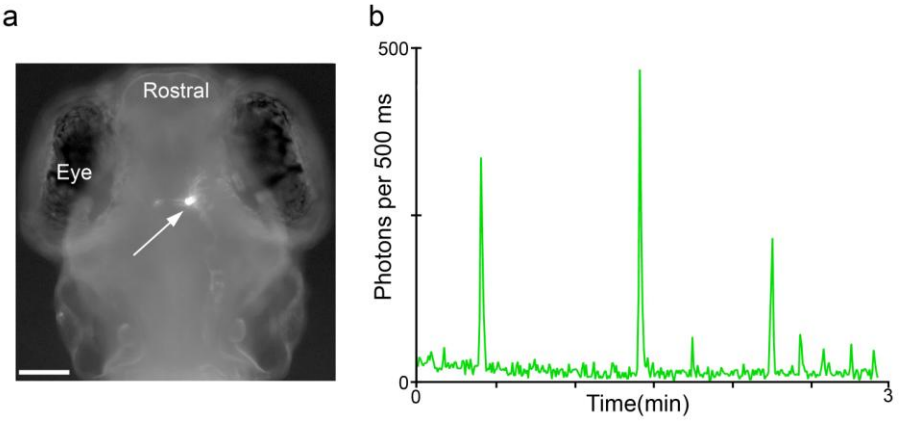

Engert_SupplementaryFigure13

Supplementary Movies

Supplementary Movie 1: Each panel displays a real-time movie (30 Hz) of a 7 dpf Nβt:GA zebrafish, previously exposed to CLZN for 24 hours, swimming freely in the neuroluminescence assay. In order to conveniently visualize neuroluminescence signals corresponding to behavior, the photons detected during each frame of the movie are plotted as green pixels in a disc surrounding the center of mass of the zebrafish image. Midway through the movie sequence, a mechanical stimulus is delivered by a computer-controlled tapping device. The stimulus time is indicated by a red circle appearing in the center of the movie frame.

Supplementary Movie 2: A neuroluminescence movie prepared similarly to that shown in Supplementary Movie 1, but displaying a zebrafish immediately (~1 minute) after exposure to PTZ.

Supplementary Movie 3: A neuroluminescence movie prepared similarly to that shown in Supplementary Movie 1, but displaying a zebrafish after prolonged exposure to PTZ (>20 minutes). Note that a brief initial swim bout is followed by a period without swimming that is corresponds with sustained neuroluminescence.

Supplementary Movie 4: A neuroluminescence movie prepared similarly to that shown in Supplementary Movie 1, but displaying a zebrafish paralyzed with α-Bungarotoxin and exposed to PTZ. The camera's zoom lens was used at full magnification, hence the reduced image quality, in order to assure that no motion was detected. Sporadic periods of sustained neuroluminescence are evident.

Supplementary Movie 5: The top row of panels display the average image acquired from a time series of two-photon images in three 5 dpf HuC:GCaMP2 zebrafish larva exposed to PTZ. The bottom row displays a movie (ten-fold accelerated) of the raw intensity images acquired during the time series. Long waves of correlated activity occur sporadically throughout the zebrafish brain.

1 Kralik, J. D. *et al.* Techniques for long-term multisite neuronal ensemble recordings in behaving animals. *Methods* **25**, 121-150 (2001).
2 Miller, E. K. & Wilson, M. A. All my circuits: using multiple electrodes to understand functioning neural networks. *Neuron* **60**, 483-488 (2008).
3 Luo, L., Callaway, E. M. & Svoboda, K. Genetic dissection of neural circuits. *Neuron* **57**, 634-660 (2008).
4 Brustein, E., Marandi, N., Kovalchuk, Y., Drapeau, P. & Konnerth, A. "In vivo" monitoring of neuronal network activity in zebrafish by two-photon Ca(2+) imaging. *Pflugers Arch.* **.** (2003).
5 Douglass, A. D., Kraves, S., Deisseroth, K., Schier, A. F. & Engert, F. Escape behavior elicited by single, Channelrhodopsin-2-evoked spikes in zebrafish somatosensory neurons. *Current Biology* **18** 1133-1137 (2008).
6 Niell, C. M. & Smith, S. J. Functional imaging reveals rapid development of visual response properties in the zebrafish tectum. *Neuron* **45**, 941-951 (2005).
7 Ramdya, P. & Engert, F. Binocular Circuit Properties Emerge Following Retinotectal Rewiring. *Nature Neuroscience* **in press** (2008).
8 O'Malley, D. M., Kao, Y. H. & Fetcho, J. R. Imaging the functional organization of zebrafish hindbrain segments during escape behaviors. *Neuron* **17**, 1145-1155 (1996).
9 Higashijima, S. I., Masino, M. A., Mandel, G. & Fetcho, J. R. Imaging neuronal activity during zebrafish behavior with a genetically encoded calcium indicator. *J.Neurophysiol.* **90**, 3986-3997 (2003).
10 Orger, M. B., Kampff, A. R., Severi, K. E., Bollmann, J. H. & Engert, F. Control of visually guided behavior by distinct populations of spinal projection neurons. *Nat.Neurosci.* **11**, 327-333 (2008).
11 McLean, D. L., Fan, J., Higashijima, S., Hale, M. E. & Fetcho, J. R. A topographic map of recruitment in spinal cord. *Nature* **446**, 71-75 (2007).
12 Gahtan, E., Sankrithi, N., Campos, J. B. & O'Malley, D. M. Evidence for a widespread brain stem escape network in larval zebrafish. *J.Neurophysiol.* **87**, 608-614 (2002).
13 Dombeck, D. A., Khabbaz, A. N., Collman, F., Adelman, T. L. & Tank, D. W. Imaging large-scale neural activity with cellular resolution in awake, mobile mice. *Neuron* **56**, 43-57 (2007).
14 Briggman, K. L., Abarbanel, H. D. & Kristan, W. B., Jr. Optical imaging of neuronal populations during decision-making. *Science* **307**, 896-901 (2005).
15 Clark, D. A., Gabel, C. V., Gabel, H. & Samuel, A. D. Temporal activity patterns in thermosensory neurons of freely moving Caenorhabditis elegans encode spatial thermal gradients. *Journal of Neuroscience* **27**, 6083-6090 (2007).
16 Baubet, V. *et al.* Chimeric green fluorescent protein-aequorin as bioluminescent Ca2+ reporters at the single-cell level. *Proc.Natl.Acad.Sci.U.S.A* **97**, 7260-7265 (2000).
17 Daunert, S. & Deo, S. K. *Photoproteins in bioanalysis*. (Wiley-VCH, 2006).
18 Smith, S. J. & Zucker, R. S. Aequorin response facilitation and intracellular calcium accumulation in molluscan neurones. *J Physiol* **300**, 167-196 (1980).
19 Ashley, C. C. & Ridgway, E. B. Simultaneous recording of membrane potential, calcium transient and tension in single muscle fibers. *Nature* **219**, 1168-1169 (1968).
20 Hastings, J. W. & Johnson, C. H. Bioluminescence and chemiluminescence. *Methods Enzymol* **360**, 75-104 (2003).
21 Shimomura, O., Musicki, B., Kishi, Y. & Inouye, S. Light-emitting properties of recombinant semi-synthetic aequorins and recombinant fluorescein-conjugated aequorin for measuring cellular calcium. *Cell Calcium* **14**, 373-378 (1993).
22 Curie, T., Rogers, K. L., Colasante, C. & Brulet, P. Red-shifted aequorin-based bioluminescent reporters for in vivo imaging of Ca2 signaling. *Mol Imaging* **6**, 30-42 (2007).

23 Martin, J. R., Rogers, K. L., Chagneau, C. & Brulet, P. In vivo bioluminescence imaging of Ca signalling in the brain of Drosophila. *PLoS ONE* **2**, e275, doi:10.1371/journal.pone.0000275 (2007).
24 Rogers, K. L. *et al.* Non-invasive in vivo imaging of calcium signaling in mice. *PLoS ONE* **2**, e974, doi:10.1371/journal.pone.0000974 (2007).
25 Rogers, K. L. *et al.* Visualization of local Ca2+ dynamics with genetically encoded bioluminescent reporters. *European Journal of Neuroscience* **21**, 597-610 (2005).
26 Cheung, C. Y., Webb, S. E., Meng, A. & Miller, A. L. Transient expression of apoaequorin in zebrafish embryos: extending the ability to image calcium transients during later stages of development. *Int J Dev Biol* **50**, 561-569 (2006).
27 Teranishi, K. & Shimomura, O. Solubilizing Coelenterazine in Water with Hydroxypropyl-Iý-cyclodextrin. *Biosci Biotechnol Biochem* **61**, 1219-1220 (1997).
28 Baraban, S. C. Emerging epilepsy models: insights from mice, flies, worms and fish. *Curr Opin.Neurol.* **20**, 164-168 (2007).
29 Tallini, Y. N. *et al.* Imaging cellular signals in the heart in vivo: Cardiac expression of the high-signal Ca2+ indicator GCaMP2. *Proc Natl Acad Sci U S A* **103**, 4753-4758, doi:0509378103 [pii]
10.1073/pnas.0509378103 (2006).
30 Park, H. C. *et al.* Analysis of Upstream Elements in the HuC Promoter Leads to the Establishment of Transgenic Zebrafish with Fluorescent Neurons. *Dev.Biol.* **227**, 279-293 (2000).
31 Sakurai, T. The neural circuit of orexin (hypocretin): maintaining sleep and wakefulness. *Nat Rev Neurosci* **8**, 171-181 (2007).
32 Prober, D. A., Rihel, J., Onah, A. A., Sung, R. J. & Schier, A. F. Hypocretin/orexin overexpression induces an insomnia-like phenotype in zebrafish. *J Neurosci* **26**, 13400-13410 (2006).
33 Yokogawa, T. *et al.* Characterization of sleep in zebrafish and insomnia in hypocretin receptor mutants. *PLoS Biol* **5**, e277, doi:07-PLBI-RA-0323 [pii]
10.1371/journal.pbio.0050277 (2007).
34 Chemelli, R. M. *et al.* Narcolepsy in orexin knockout mice: molecular genetics of sleep regulation. *Cell* **98**, 437-451 (1999).
35 Lin, L. *et al.* The sleep disorder canine narcolepsy is caused by a mutation in the hypocretin (orexin) receptor 2 gene. *Cell* **98**, 365-376 (1999).
36 Mileykovskiy, B. Y., Kiyashchenko, L. I. & Siegel, J. M. Behavioral correlates of activity in identified hypocretin/orexin neurons. *Neuron* **46**, 787-798 (2005).
37 Lee, M. G., Hassani, O. K. & Jones, B. E. Discharge of identified orexin/hypocretin neurons across the sleep-waking cycle. *J Neurosci* **25**, 6716-6720 (2005).
38 Adamantidis, A. R., Zhang, F., Aravanis, A. M., Deisseroth, K. & de Lecea, L. Neural substrates of awakening probed with optogenetic control of hypocretin neurons. *Nature* **450**, 420-424 (2007).
39 Mank, M. & Griesbeck, O. Genetically Encoded Calcium Indicators. *Chem.Rev.* **108**, 1550-1564 (2008).
40 Tricoire, L. *et al.* Calcium dependence of aequorin bioluminescence dissected by random mutagenesis. *Proc Natl Acad Sci U S A* **103**, 9500-9505, doi:0603176103 [pii]
10.1073/pnas.0603176103 (2006).
41 Roncali, E. *et al.* New device for real-time bioluminescence imaging in moving rodents. *J Biomed Opt* **13**, 054035, doi:10.1117/1.2976426 (2008).
42 Drobac, E., Tricoire, L., Chaffotte, A. F., Guiot, E. & Lambolez, B. Calcium imaging in single neurons from brain slices using bioluminescent reporters. *J Neurosci Res*, doi:10.1002/jnr.22249 (2009).
43 Pologruto, T. A., Yasuda, R. & Svoboda, K. Monitoring neural activity and [Ca2+] with genetically encoded Ca2+ indicators. *J Neurosci* **24**, 9572-9579, doi:24/43/9572 [pii]

10.1523/JNEUROSCI.2854-04.2004 (2004).
44 Scott, E. K. *et al.* Targeting neural circuitry in zebrafish using GAL4 enhancer trapping. *Nat Methods* **4**, 323-326 (2007).
45 Lillesaar, C., Tannhauser, B., Stigloher, C., Kremmer, E. & Bally-Cuif, L. The serotonergic phenotype is acquired by converging genetic mechanisms within the zebrafish central nervous system. *Dev Dyn* **236**, 1072-1084 (2007).
46 Wen, L. *et al.* Visualization of monoaminergic neurons and neurotoxicity of MPTP in live transgenic zebrafish. *Dev Biol* **314**, 84-92 (2008).
47 Zhang, F. *et al.* Multimodal fast optical interrogation of neural circuitry. *Nature* **446**, 633-639 (2007).
48 Deisseroth, K. *et al.* Next-generation optical technologies for illuminating genetically targeted brain circuits. *Journal of Neuroscience* **26**, 10380-10386 (2006).
49 Plautz, J. D., Kaneko, M., Hall, J. C. & Kay, S. A. Independent Photoreceptive Circadian Clocks Throughout Drosophila. *Science* **278**, 1632-1635 (1997).
50 Flusberg, B. A. *et al.* High-speed, miniaturized fluorescence microscopy in freely moving mice. *Nat.Methods* **5**, 935-938 (2008).